

Sequential clustering reactions of Si⁺ with SiD₄: Identification of a bottleneck preventing rapid growth of hydrogenated silicon particles

M. L. Mandich, W. D. Reents Jr., and M. F. Jarrold

Citation: *The Journal of Chemical Physics* **88**, 1703 (1988); doi: 10.1063/1.454737

View online: <http://dx.doi.org/10.1063/1.454737>

View Table of Contents: <http://scitation.aip.org/content/aip/journal/jcp/88/3?ver=pdfcov>

Published by the [AIP Publishing](#)

Articles you may be interested in

[Evidence for coupling of Si–Si lattice vibration and Si–D wagging vibration in deuterated amorphous silicon](#)
Appl. Phys. Lett. **74**, 3347 (1999); 10.1063/1.123340

[Sequential reactions of SiD⁺ 2 with SiD₄](#)
J. Chem. Phys. **96**, 4429 (1992); 10.1063/1.462834

[Sequential clustering reactions of SiD⁺ with SiD₄: Rapid growth to kinetic deadend structures](#)
J. Chem. Phys. **95**, 7360 (1991); 10.1063/1.461362

[Sequential clustering reactions of SiD⁺ 3 with SiD₄ and SiH⁺ 3 with SiH₄: Another case of arrested growth of hydrogenated silicon particles](#)
J. Chem. Phys. **92**, 437 (1990); 10.1063/1.458446

[Sequential reactions of bare silicon clusters with SiD₄: Constrained heterogeneous nucleation of deuterated silicon particles](#)
J. Chem. Phys. **90**, 3121 (1989); 10.1063/1.456667



Sequential clustering reactions of Si^+ with SiD_4 : Identification of a bottleneck preventing rapid growth of hydrogenated silicon particles

M. L. Mandich, W. D. Reents, Jr., and M. F. Jarrold
AT&T Bell Laboratories, Murray Hill, New Jersey 07974

(Received 21 August 1987; accepted 15 October 1987)

Sequential clustering of atomic silicon-29 cations with SiD_4 is observed at room temperature in the ion cell of a Fourier transform mass spectrometer. The clustering reactions proceed in a highly specific fashion. Si^+ grows initially by sequential addition of three $-\text{SiD}_2$ units. The measured reaction rates for these three steps are, respectively, 8.1 ± 0.4 , 0.36 ± 0.04 , and $2.0 \pm 0.3 \times 10^{-10} \text{ cm}^3 \text{ molecule}^{-1} \text{ s}^{-1}$. A back reaction which results in loss of the silicon-29 isotopic label also occurs for these three reactions and represents $\sim 12\%$ – 15% of the reaction products, depending on the reaction step. This cluster growth mechanism then encounters a critical bottleneck and ceases. Further aggregation occurs only by slow bimolecular attachment of SiD_4 at a rate of $1.0 \pm 0.3 \times 10^{-13} \text{ cm}^3 \text{ molecule}^{-1} \text{ s}^{-1}$ at $p(\text{SiD}_4) = 2.0 \times 10^{-7}$ Torr. The fundamental mechanisms and energetics for the individual reaction pathways have been calculated by Raghavachari using *ab initio* electronic structure theory and are presented in a companion paper. The clustering mechanism involves insertion of a cluster ion into a SiD bond of SiD_4 followed by elimination of D_2 . Addition of $-\text{SiD}_2$ serves to increasingly saturate the bonds of all of the silicon centers which leads to the observed growth limitations at Si_4D_6^+ . The accuracy of these calculated potential surfaces is tested using statistical phase space theory. Since both the forward and reverse reaction rates are measured using isotopic labeling, the phase space theory calculations are used to determine both the insertion and the elimination transition state energies for each of the first three clustering steps as well as a lower limit for the well depth of the $[\text{Si}_5\text{D}_{10}^+]$ intermediate complex. Overall, good agreement is found between the transition state energies obtained from phase space theory and those determined by Raghavachari. These results indicate that Si^+ clustering with SiD_4 encounters an early bottleneck which prevents rapid formation of the critical nucleus size required for spontaneous growth of large hydrogenated silicon particulates.

I. INTRODUCTION

Condensation nuclei have long been known to promote extremely rapid heterogeneous nucleation and growth of gas phase particles.¹ This phenomenon is widely exploited in some cases including cloud seeding, aerosol generation, and liquification of gases, but poses serious problems in others, for example, conditions leading to smog, steam turbine performance, and chemical vapor deposition processes. In gross theoretical terms, these particle embryos increase the rate of nucleation by lowering the free energy of formation of the prenucleation cluster required for diffusion controlled growth. More precise treatments of this effect have been hindered because of the paucity of information about chemical and physical properties of condensation nuclei.

One example of undesirable particulate formation is the occurrence of hydrogenated silicon dust during silane chemical vapor deposition of silicon films.² This problem arises particularly when large deposition rates are attempted, resulting in low silicon film quality and nonproductive gas consumption.³ Considerable experimental and theoretical work has been directed over the past two decades towards understanding the gas phase chemistry of silane chemical vapor deposition.⁴ More recently, Kushner has developed a kinetic model describing silicon particulate formation based on rapid, unlimited polymerization of SiH_n radicals with other silane species.⁵ This model emphasizes that chemical

reactions are required in order to form a critical nucleus size which then proceeds to grow spontaneously. The difficulty lies in identifying just which of the many possible reactants and reactions are central to this process. The reason for this is simple: *there is a severe lack of hard data for the rates and products of sequential clustering reactions which lead to the formation of larger particles.*

Ion-molecule clustering reactions are ideally suited for studying the processes by which condensation nuclei form and have been used to study neutral clustering about ions⁶ and aggregation of large transition metal carbonyls.^{7–10} This paper describes the detailed information that we have obtained about the individual steps of the sequential ion-molecule clustering reactions of ground state $^{29}\text{Si}^+$ with SiD_4 . Overall, clustering proceeds by stepwise addition of $-\text{SiD}_2$ accompanied by loss of D_2 . A crucial bottleneck occurs following formation of Si_4D_6^+ . The previous mechanism suddenly switches off and further growth happens only by slow attachment of SiD_4 . The mechanism and energetics for each reaction pathway have been derived by Raghavachari using *ab initio* electronic structure theory.¹¹ The mechanisms for the clustering reactions involve $\text{Si}-\text{D}$ bond insertion, accompanied by $\text{Si}-\text{Si}$ bond formation which follows well-established silicon chemistry.¹² These *ab initio* calculations are qualitatively consistent with the observed clustering sequence and explain the abrupt halt of $-\text{SiD}_2$ addition at

Si₄D₆⁺. In turn, we have quantitatively tested the accuracy of the calculated potential surfaces using statistical phase space theory developed by Chesnavich and Bowers.¹³ In our experiments, we are able to measure the reaction rates for both the forward and the reverse reactions with silicon-29 isotopic labeling of the reactants. This permits us to use the phase space theoretical model to critically determine the energy of the two highest transition states along the reaction coordinate for each clustering step. Overall, good agreement is found between the transition state energies obtained from our phase space calculations based on our experimental data and those calculated by Raghavachari.

II. EXPERIMENTAL METHOD

Sequential reactions of ²⁹Si⁺ ions with SiD₄ are studied in the trapped ion cell of a modified Nicolet FT/MS-1000 Fourier transform mass spectrometer (FTMS).^{14,15} As has been previously described, silicon atomic ions are created by laser evaporation of a bulk silicon target located just outside of the low pressure side of a differentially pumped FTMS dual ion cell.¹⁶ Silicon-29 isotopically labeled ions are selected from the total silicon atomic ion population using standard double resonance techniques.¹⁷ SiD₄ (MSD Isotope Co., Inc., 99.7 at. % enriched in deuterium as determined by our mass spectral analysis; used without further purification) is introduced into the "high pressure" side of the dual ion cell. The exothermic ion-molecule reactions of ²⁹Si⁺ with SiD₄ are then monitored by recording the mass spectra of the ions in the cell over a sequence of reaction times.

Other conditions in these experiments include the following. The pulsed Nd:YAG (Quanta-Ray DCR-2) laser is operated at 532 nm at a typical energy of 5–10 mJ/pulse and focused to a spot size of about 0.2 mm diameter. The FTMS is operated with a solenoid magnetic field strength of 2.96 T, trapping potentials of +1.00 V, 32 K data points, signal averaging of 100 spectra, and trapping times of 0–1000 ms. Typical SiD₄ pressures are 0.4–4 × 10⁻⁶ Torr as measured by a Bayard-Alpert ion gauge located over the diffusion pump. Corresponding true pressures of 0.2–2 × 10⁻⁶ Torr are estimated from corrections for the ion gauge sensitivity and instrumental factors as previously described using the proton transfer rate for CH₄ as a known calibration rate.^{16,18–20} Elemental compositions of reactant and product ions were obtained by measuring their masses and comparing each to its calculated exact mass. The experimentally determined masses were found to be within 10 ppm of the exact masses, thus verifying their stoichiometries.

III. RESULTS

Sequential clustering of ²⁹Si⁺ with SiD₄ is observed, starting with ²⁹Si⁺ and terminating with Si₅D₁₀⁺. The intensities of the evolving ion populations are shown as a function of time in Figs. 1–3, with the exception of Si₅D₁₀⁺. The Si₅D₁₀⁺ is formed quite slowly; therefore, its intensity is monitored in separate experiments at longer reaction times.²¹ For simplicity, all subsequent references to ionic and neutral species containing one silicon-29 atom will be denoted as *Si_xD_y, e.g., ²⁹Si⁺ ≡ *Si⁺, and ²⁹Si²⁸Si₂D₄⁺ ≡ *Si₃D₄⁺.

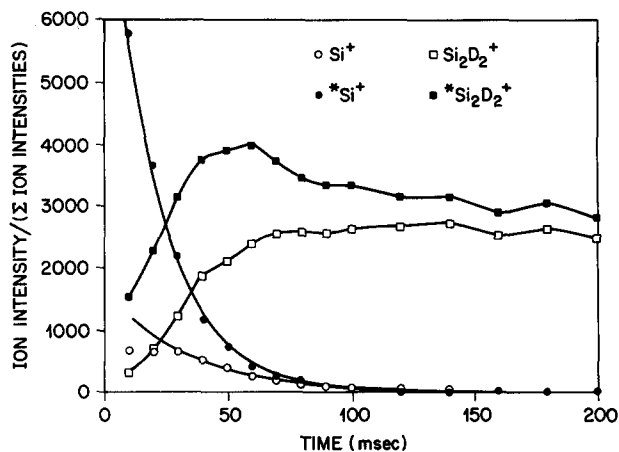
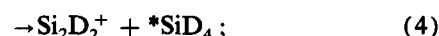
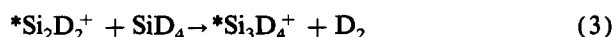


FIG. 1. Time evolution of the initial reactant *Si⁺ population during reaction with 1.85 × 10⁻⁶ Torr of SiD₄. The time dependences of its two primary product ions, Si⁺ and *Si₂D₂⁺, are depicted along with the secondary product ion, Si₂D₂⁺ which is formed by both of the primary product ions. Ion intensities have been corrected for isotopic abundance and normalized to the total ion intensity in the cell. The smooth line through the data points for *Si⁺ is the fit to a pseudo-first-order decay which yields the rate constant in Table I. The smooth line through the Si⁺ data also represents the fit to a pseudo-first-order decay. The lines through the *Si₂D₂⁺ and Si₂D₂⁺ data points are only present as a guide and do not represent theoretical fits.

In the first three clustering reactions, a branching is observed between formation of products and isotopic exchange with the SiD₄ reagent;



and

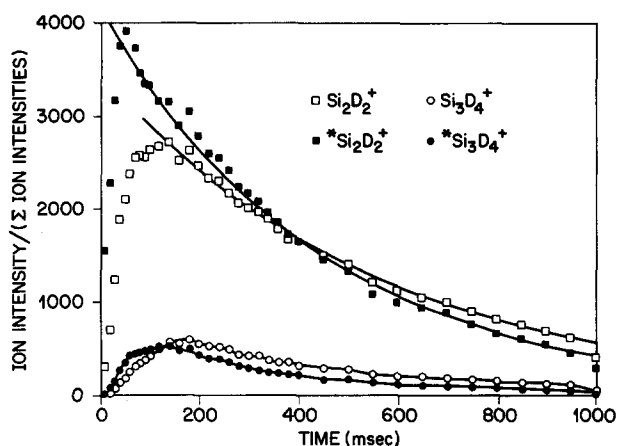


FIG. 2. Time evolution of the second reactant *Si₂D₂⁺ ion population in the sequential cluster reactions with SiD₄. The time dependences of its two primary product ions, *Si₃D₄⁺ and Si₂D₂⁺, are also shown; Si₂D₂⁺ is also formed by Si⁺. The time dependence of a secondary product ion, Si₃D₄⁺ which is formed from *Si₃D₄⁺ as well as Si₂D₂⁺ is depicted. Ion intensities have been corrected for isotopic abundances and normalized to the total ion population in the cell. The smooth lines through the data points for *Si₂D₂⁺ indicate the fit to a pseudo-first-order decay which gives the reaction rate constant presented in Table I. A similar fit is drawn through the data points for Si₂D₂⁺. The line through *Si₃D₄⁺ and Si₃D₄⁺ data points serve only as a guide and do not represent curve fits. Note the suppressed intensity of both the labeled and unlabeled Si₃D₄⁺ species. This occurs because these ions react away at a rate which is greater than their formation rate (cf. Table I).

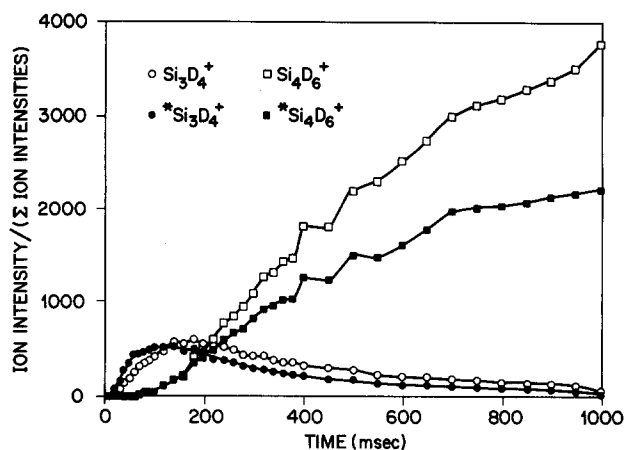
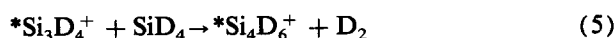


FIG. 3. Formation and decay of the third reactant, $^*\text{Si}_3\text{D}_4^+$, in the sequential clustering reactions with SiD_4 along with its primary products, $^*\text{Si}_4\text{D}_6^+$ and Si_3D_4^+ . The latter unlabeled species is also formed by Si_2D_2^+ and reacts to form Si_4D_6^+ which in turn is also formed as a secondary product via $^*\text{Si}_4\text{D}_6^+$. The ion populations have been corrected for isotopic abundances and normalized to the total ion population residing in the ion cell. None of the curves through the data points represent mathematical fits to the data and are only there as a guide. Note that the product ions, $^*\text{Si}_4\text{D}_6^+$ and Si_4D_6^+ , are much more intense than the labeled and unlabeled Si_3D_4^+ ions from which they originate. This occurs because the decay rate of both labeled and unlabeled Si_3D_4^+ is much more rapid than its formation rate; subsequent decay of Si_4D_6^+ is also quite slow.



The fourth clustering reaction terminates the reaction sequence observed during the time scale of these experiments²¹:



Once formed, the unlabeled Si^+ , Si_2D_2^+ , etc. ions react iden-

tically to their silicon-29 labeled counterparts, except that the reverse process involving isotopic exchange can no longer be monitored.

A kinetic analysis of the exponential rise and fall of each ion is performed to determine their formation and decay rates. The rates for $^*\text{Si}^+/\text{Si}^+$ and $^*\text{Si}_2\text{D}_2^+/\text{Si}_2\text{D}_2^+$ are determined from the exponential decay of the normalized reactant ion intensity vs time. In reactions with SiD_4 , the $^*\text{Si}_3\text{D}_4^+/\text{Si}_3\text{D}_4^+$ ions have a larger rate constant than the $^*\text{Si}_2\text{D}_2^+/\text{Si}_2\text{D}_2^+$ ions which form them. Therefore, steady state approximations are appropriate for extracting decay rates from the time dependent $^*\text{Si}_3\text{D}_4^+$ and Si_3D_4^+ populations. The reaction rate for the final attachment reaction, Eq. (7), is obtained from a comparison of the reactant and product ion intensities before and after a known reaction time.²¹ Si_4D_6^+ is allowed to form and then is isolated by double resonance ejection of all other trapped ions in the cell. After a suitable reaction time, Δt , the intensities of the reactant and product ions are measured. Additional double resonance ejection confirms that one product is formed, $\text{Si}_5\text{D}_{10}^+$, which comes only from Si_4D_6^+ . Therefore, the rate for this reaction, k , is given by

$$k = \frac{-\ln\{[\text{Si}_4\text{D}_6^+]/([\text{Si}_4\text{D}_6^+] + [\text{Si}_5\text{D}_{10}^+])\}}{[\text{SiD}_4]\Delta t} \quad (8)$$

All decays are single exponential and scale linearly with pressure. Note that those species with the silicon-29 isotope have somewhat different kinetic behavior than the corresponding ions which have lost the isotopic labeling. This occurs because the formation of the nonisotopically labeled ions is essentially irreversible and contributes to the overall decay rate of the labeled ion. This is not the case for the unlabeled species. When this is taken into account, good agreement is reached between the formation and decay rates

TABLE I. Sequential clustering reactions of $^{29}\text{Si}^+$ with SiD_4 .

Reaction ^a	Product fraction (%)	Rate constant ^b ($\times 10^{10}$) ($\text{cm}^3 \text{ molecule}^{-1} \text{ s}^{-1}$)	Reaction probability ^c
$^*\text{Si}^+ + \text{SiD}_4 \rightarrow ^*\text{Si}_2\text{D}_2^+ + \text{D}_2$ ^{d,e}	85 ± 4	8.1 ± 0.4 ^f	0.66 ± 0.04
$\text{Si}^+ + ^*\text{SiD}_4$ ^c	15 ± 4		
$^*\text{Si}_2\text{D}_2^+ + \text{SiD}_4 \rightarrow ^*\text{Si}_3\text{D}_4^+ + \text{D}_2$	88 ± 5	0.36 ± 0.04	0.035 ± 0.004
$\text{Si}_2\text{D}_2^+ + ^*\text{SiD}_4$	12 ± 5		
$^*\text{Si}_3\text{D}_4^+ + \text{SiD}_4 \rightarrow ^*\text{Si}_4\text{D}_6^+ + \text{D}_2$	87 ± 5	2.0 ± 0.3	0.21 ± 0.03
$\text{Si}_3\text{D}_4^+ + ^*\text{SiD}_4$	13 ± 5		
$\text{Si}_4\text{D}_6^+ + \text{SiD}_4 \rightarrow \text{Si}_5\text{D}_{10}^+$ ^g	100	0.0010 ± 0.0003 ^h	0.000 11 ± 0.000 03 ^h

^a Only exothermic reactions are given here. See Ref. 25 for a description of the various endothermic reactions and reaction products that have also been observed in our studies. Neutral products are given based on thermodynamical calculations of possible products. Those species which contain one silicon-29 isotope are designated as $(^*\text{Si}_x\text{D}_y)^{(+)}$. For example, $^*\text{Si}_5\text{D}_{10}^+ \equiv ^{29}\text{Si}^{28}\text{Si}_4\text{D}_{10}^+$.

^b The rate constant is the total measured reaction rate for the silicon-29 labeled species and includes isotopic exchange where observed.

^c The probability of reaction is calculated as the ratio of the measured reaction rate to the Langevin ion-molecule collision rate K_L ; see Eq. (20).

^d This exothermic reaction product has been previously reported in ion cyclotron resonance and low energy ion beam studies of the reactions of Si^+ with SiD_4 and SiH_4 ; Refs. 22 and 23.

^e This isotopic exchange process has been observed in low energy ion beam studies of the reactions of Si^+ with SiD_4 and SiH_4 ; Ref. 23. In ion beam work, however, the isotopic exchange has been reported to be endothermic. Our experimental findings are not consistent with this process being endothermic at room temperature. This discrepancy is analyzed further in Sec. V A.

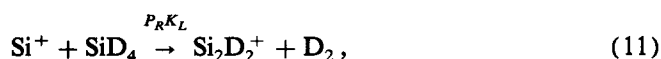
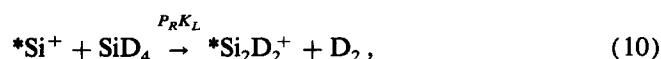
^f This rate constant has also been previously determined (Refs. 22 and 23) and the afore determined values are consistent with our measurements when consistent reference pressure calibrations are used and the isotopic exchange process is properly accounted for.

^g Only unlabeled Si_4D_6^+ reactions have been examined.

^h Measured at $p(\text{SiD}_4) = 2.0 \times 10^{-7}$ Torr.

of the labeled and unlabeled ions. Table I summarizes the decay rates for each of the reactions of the *silicon-29 isotopically labeled* ions in the clustering sequence given in reactions (1), (3), (5), and (7).^{22,23}

The kinetic behavior of the labeled and unlabeled ions are also used to determine the product distributions for each step of the clustering process. In principle, the product branching ratios can be obtained from the direct ratio of the product ion intensities. However, the first clustering step produces appreciable amounts of unlabeled Si⁺ which reacts in parallel with *Si⁺ but produces only unlabeled Si₂D₂⁺. This unlabeled Si₂D₂⁺, plus the contribution from the isotopic exchange in the second clustering step, in turn reacts again to form unlabeled Si₃D₄⁺, etc. Thus, it becomes increasingly difficult to deconvolute the various contributions to the unlabeled product ion populations. Alternatively, the decay rates of the labeled vs the total reactant ions can be used to obtain the product ratios. Using the reaction of *Si⁺/Si⁺ as an example, this analysis is as follows (where K_L is the ion-molecule collision rate; P_E and P_R are the probability for isotopic exchange and reaction, respectively):



$$\frac{d[*Si^+]}{dt} = -P_E K_L [*Si^+][SiD_4] - P_R K_L [*Si^+][SiD_4], \quad (12)$$

$$\frac{d\{[*Si^+] + [Si^+]\}}{dt} = -P_R K_L [SiD_4]\{[*Si^+] + [Si^+]\}. \quad (13)$$

The product fraction of *Si₂D₂⁺ is thus given by the decay rate for the total Si⁺ population divided by the decay rate for the *Si⁺ population. A similar analysis is performed to obtain the product ratios given in Table I for the other clustering reactions.

Particular care is taken to determine the reaction rates and products for the thermalized ground state ion populations and distinguish them from those which have resulted from the reactions of ions which contained excess energy. This is accomplished by several means. First, the reaction rates are sufficiently slow (except for ²⁹Si⁺) that it is possible to analyze only those products which are formed after a delay which allows for thermalizing collisions. This is done for each reaction in the sequence by double resonance ejection of the presumed products during the course of each reaction. The remaining reactant ions are allowed to continue to react and the products are measured as a function of the delay time before the ejection. This analysis indicates, e.g., that 5–10 collisions are required to remove excess energy from Si₂D₂⁺ and 10–15 collisions are sufficient to relax Si₃D₄⁺. These collisional deactivation rates are reasonable when compared to the limited data that is available for elec-

tronic and vibrational relaxation rates of molecular ions.²⁴ Second, those products which are formed from excited ions can often be identified since they appear unusually early in the reaction of a particular species and show nonexponential kinetic behavior. The formation of these “hot” ion products account for the slight deviations of the data at early times from the superimposed fits in Figs. 1 and 2. Quantitative correction of the reactant ion intensities for formation of these products expunges all deviations from a pseudo-first-order decay. Third, several of the excited ion reactions can be distinguished by their inordinate sensitivity to factors such as the laser evaporation power, the magnitudes of the rf power used for either the double resonance or detection excitations, and reagent pressure. Our studies of the reactions of these excited ²⁹Si⁺ and Si_xD_y⁺ have yielded fascinating results which are outside the scope of the work presented here.²⁵ In summary, it has been possible to measure reaction rates and product distributions for ground state species which are equilibrated with the cell wall temperature of 300 K.

IV. THEORY

The experimental evidence demonstrates unequivocally that the clustering of ²⁹Si⁺ with SiD₄ proceeds in a highly specific fashion. Overall, the cluster grows by addition of three –SiD₂ units. Then, on the time scale of these experiments, the cluster reaches a terminal size after bimolecular attachment of SiD₄. Furthermore, three of the steps in the clustering process show isotopic exchange of the labeled silicon-29 with SiD₄. This indicates that the silicon atom from the neutral reagent, SiD₄, becomes equivalent to at least one of the silicon atoms in the growing cluster at some point along the reaction coordinate.

The mechanisms and energetics of the reaction pathways for the sequential clustering reactions have been determined by Raghavachari using *ab initio* electronic structure calculations and are described in his companion paper.¹¹ Qualitatively, these mechanisms accurately describe cluster growth by reaction with SiD₄ to add –SiD₂ and eliminate D₂. Furthermore, the mechanisms explain why addition of –SiD₂ terminates with formation of Si₄D₆⁺ and why further reaction occurs only via bimolecular attachment of SiD₄ to Si₄D₆⁺ forming Si₅D₁₀⁺. The accessible intermediates which allow for the isotopic exchange of silicon-29 are also qualitatively predicted by these mechanisms.

We have also *quantitatively* compared our experimental results to the calculated energetics of Raghavachari's potential surfaces for each clustering step using statistical phase space theory. Our phase space calculations use molecular constants derived by Raghavachari for the various reaction intermediates to derive reaction rates and isotopic exchange probabilities as a function of several key energies along the potential surface. These transition state/intermediate complex energies are used as adjustable parameters in order to fit the phase space theoretical results to our experimentally measured reaction rates and product fractions. In particular, our observation of both the reactive and nonreactive (isotopic exchange) channels provides a sensitive test for several of the important microscopic details of the calculated reaction

potential surfaces. Good agreement is found between the transition state energies obtained from our theoretical phase space model and those calculated by Raghavachari, Table II. The reaction mechanisms and phase space model calculations are described below for each step of the cluster process.²⁶

A. Si⁺ + SiD₄

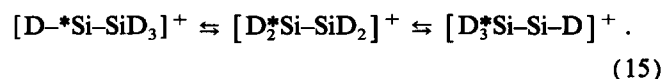
The potential surface for the first step of the clustering reaction is shown in Fig. 4. The reaction starts with formation of a [^{*}Si⁺⋯(SiD₄)] complex, C1, where the two silicon centers sandwich either one or two bridging deuterium atoms.¹¹ The binding energy of this hydrogen bonded complex as determined by *ab initio* electronic structure calculations is much larger than would be expected for a complex bound purely by attractive ion–molecule forces. For comparison, the ion–molecule binding energy of the structure with two bridging deuteriums can be determined from the familiar expression for the electrostatic polarization energy, $V_{\text{ion-dipole}}$ produced by the interaction of a point charge with a polarizable molecule that does not have a dipole moment²⁷;

$$V_{\text{ion-dipole}} = -\frac{\alpha e^2}{2R^4}. \quad (14)$$

The factor e is the unit charge of the Si⁺ ion. α is the polarizability which is calculated from the average parallel and per-

pendicular bond polarizabilities of the Si–D bonds of SiD₄ at a mean distance R , of each bond to the Si⁺ ionic charge.^{19,28} Using the Hartree–Fock optimized geometry for the double bridged structure, C1, to estimate the bonding distances of a hypothetical ion–molecule complex yields an electrostatic polarization energy of only -0.48 eV as compared to the *ab initio* calculated energy for this complex of -1.0 eV.¹¹ A similar calculation performed for the complex with a single bridging deuterium yields an electrostatic binding energy of only -0.24 eV. Note that the ion–induced dipole energies calculated from the C1 geometries must be considered to be lower limits since the SiD₄–Si⁺ distances are clearly short enough to allow covalent interactions; this is counter to the assumption of pure electrostatic attraction implied by Eq. (14).

Following formation of the hydrogen bridged complex, ^{*}Si⁺ inserts into an Si–D bond of SiD₄, to give the reaction intermediate [D–^{*}Si–SiD₃]⁺, C2. Formation of the reaction product, D₂^{*}Si₂⁺, ensues by elimination of D₂ from the [D–^{*}Si–SiD₃]⁺ intermediate. Alternatively, [D–^{*}Si–SiD₃]⁺ can undergo a reversible 1,2 hydrogen shift to form the symmetric intermediate, [D₂^{*}Si–SiD₂]⁺, C3. It is in the [D₂^{*}Si–SiD₂]⁺ intermediate that scrambling of the silicon-29 isotope occurs,



Note that once C2 is formed, C3 can be readily formed as well because it is energetically quite accessible from [D–^{*}Si–SiD₃]⁺ and the reaction complex contains more than enough energy to overcome the transition state at TS3.

The isotopic scrambling in Eq. (15) has two effects. The first result is that the product ions D₂^{*}Si₂⁺ consist of a mixture of the two isotopically labeled species, [D₂^{*}Si–Si⁺] and [D₂Si–^{*}Si⁺], which are noninterconverting.¹¹ Second, it enables formation of unlabeled Si⁺ via the back reaction described by Eq. (2). In our experiments, this back reaction is observed to compete with ^{*}Si₂D₂⁺ product formation on an equivalent time scale (Fig. 1). This supports the mechanism for isotopic exchange described above and in Fig. 4: isotopic exchange occurs along a microscopic pathway which is common to that leading to Si₂D₂⁺ product formation and reflects an intrinsic barrier in the exit channel. This barrier causes some of the reaction intermediates to go back out the entrance channel which results in the observed isotopic exchange.

In order to quantitatively compare our experimentally derived reaction probabilities with the energetics shown in the potential surface for the ^{*}Si⁺ + SiD₄ reaction (Fig. 4) it is necessary to calculate the reaction dynamics along this surface. We use a phase space transition state theoretical model (PST) as applied to ion–molecule interactions which has been developed by Chesnavich and Bowers.¹³ An orbiting transition state, TS0, is assumed in the entrance channel and the other salient transition states, TS1, TS2, and TS3, are considered to be tight.¹³ The orbiting transition state, TS0', in the exit channel is neglected given the exothermicity of this reaction.

The first quantity that can be calculated and compared

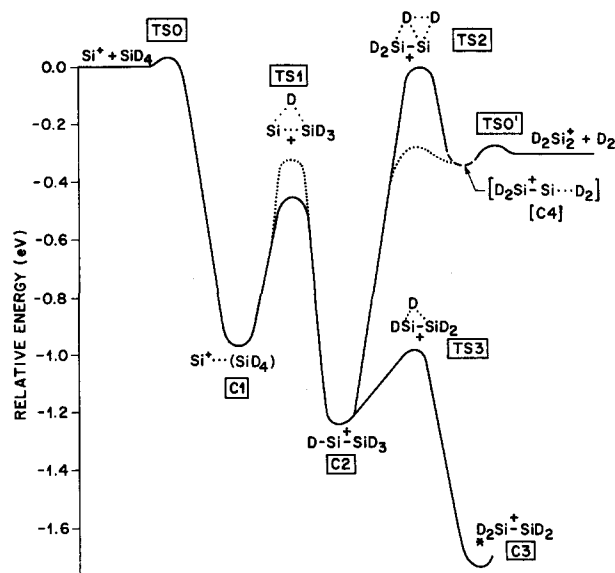


FIG. 4. Schematic potential energy surface depicting the important intermediates, C(1–4), and transition states, TS(0–3), in the reaction of Si⁺ with SiD₄. The symmetric structure, C3, where scrambling of the silicon-29 isotope can occur is highlighted by a star [cf. Eq. (15)]. All of the energies for the products, reactants, C(*i*), and TS(*i*) which are obtained from the *ab initio* electronic structure calculations in Ref. 11 are indicated by solid lines. The orbiting transition states, TS0 and TS0', in the entrance and exit channels are depicted by solid lines through the average (Boltzmann) energy of these states at 300 K. The dashed line at C4 and brackets around the depicted C4 structure indicate that this structure and energy were estimated. Dotted lines at TS1 and TS2 show the energies calculated for these transition states using the PST model which are consistent with the experimental measurements of this work. Zero-point energies (for Si/D species) are included; all energies are relative to the energy of the Si⁺/SiD₄ reactants which is set to zero. The shape of the lines connecting the various energies is not intended to represent a true potential contour.

directly to experiment is the branching ratio I_E/I_R of isotopic exchange [Eq. (2)] relative to formation of $^*\text{Si}_2\text{D}_2^+$ [Eq. (1)]. In order to calculate this quantity using phase space theory, it is assumed that there is a 50% probability of isotopic exchange during the time the reaction complex passes through the $[\text{D-}^*\text{Si}_2\text{D}_3]^+$ intermediate (C2). This assumption is reasonable since the barrier for the exchange process is quite low relative to the other barriers in the reaction and kinetic isotope effects favoring one particular position of the silicon-29 isotope in TS3 will be negligible (see below). The probabilities for formation of $^*\text{Si}_2\text{D}_2^+$ and isotopic exchange at an initial energy E and rotational angular momentum J are given by $\omega_1(E, J)$ and $\omega_2(E, J)$, respectively. Details on the explicit expressions for and derivations of $\omega_i(E, J)$ can be found in the Appendix.

The macroscopic observables are related to the total probabilities, $\omega_i(T)$. These are obtained from the microcanonical probabilities, $\omega_i(E, J)$ by averaging over the Boltzmann distribution of energies of the reactants at the reaction temperature ($T = 300$ K) and allowed values of the total rotational angular momentum, normalized to the total flux F_0 through the reaction entrance channel at TS0:

$$\omega_i(T) = \frac{\int_0^\infty dE e^{-E/kT} \int_0^{J_{\text{MAX}}} dJ 2J F_0(E, J) \omega_i(E, J)}{\int_0^\infty dE e^{-E/kT} \int_0^{J_{\text{MAX}}} dJ 2J F_0(E, J)} \quad (16)$$

The observed branching ratio can be obtained by a ratio of total probabilities $\omega_i(T)$;

$$\frac{I_E}{I_R} = \frac{\omega_2(T)}{\omega_1(T)} \quad (17)$$

The overall reaction probability of $^*\text{Si}^+$ is the second quantity that can be calculated and compared to our experimentally observed value. The decay of $^*\text{Si}^+$ that we calculate includes both loss due to isotopic exchange and production of $^*\text{Si}_2\text{D}_2^+$. The decay rate constant of $^*\text{Si}^+$, $K_{^*\text{Si}^+}(T)$, is given by

$$K_{^*\text{Si}^+}(T) = \frac{F_0(T) [\omega_1(T) + \omega_2(T)]}{\rho_R} \quad (18)$$

$\omega_1(T)$ and $\omega_2(T)$ are the thermal probabilities for isotopic exchange and formation of $^*\text{Si}_2\text{D}_2^+$, respectively, as described in the previous paragraph. The remaining factor in the numerator of Eq. (18), $F_0(T)$, is the total thermal flux through the orbiting transition state TS0, averaged over E and J ;

$$F_0(T) = \int_0^\infty dE e^{-E/kT} \int_0^{J_{\text{MAX}}} dJ 2J F_0(E, J) \quad (19)$$

ρ_R is the reactant density of states. Note that in Eq. (18), $F_0(T)/\rho_R$ is just the Langevin rate K_L ,

$$K_L = 2\pi q [\alpha/\mu]^{1/2} \\ = 1.22 \times 10^{-9} \text{ cm}^3 \text{ molecule}^{-1} \text{ s}^{-1} \text{ for } ^*\text{Si-SiD}_4 \text{ collisions,} \quad (20)$$

where q is the ionic charge, α is the molecular polarizability (4.339 \AA^3 for SiD_4 ^{19,28}), and μ is the reduced mass of the collision pair.

The PST calculations of the isotopic exchange fraction

$[I_E/(I_E + I_R)]$ and reaction probability for $^*\text{Si}^+$, $[K_{^*\text{Si}^+}(T)/K_L]$, are plotted in Figs. 5(a) and 5(b) over reasonable values for TS1 and TS2. The experimental values are superimposed which shows the allowed ranges of TS2 for a given TS1. Overall, the reaction probability is more sensitive to the height of the insertion transition state barrier TS1, whereas the fraction of isotopic exchange is more sensitive to the height of the elimination transition state barrier at TS2. Neither the experimentally measured isotopic exchange

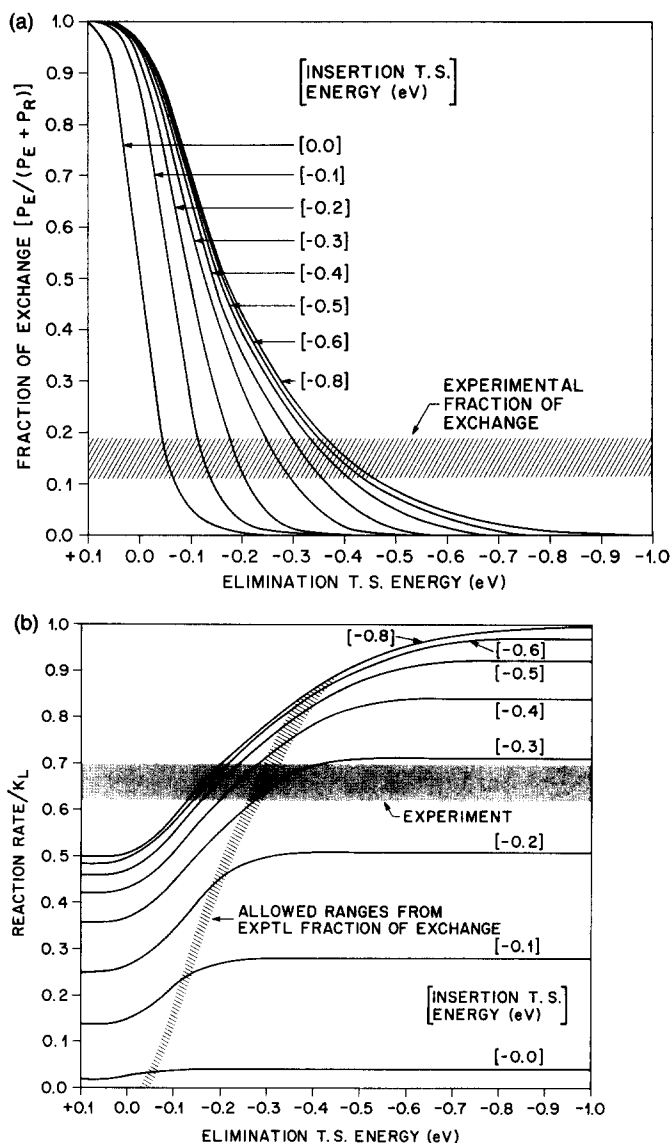


FIG. 5. PST model calculations for the reaction of Si^+ with SiD_4 , Eqs. (1) and (2), over a range of the insertion and elimination transition states energies (TS1 and TS2, Fig. 4). (a) The fraction of isotopic exchange, derived from Eq. (17), of the total products for this reaction as a function of TS1 and TS2. Curves for TS1 energies of less than -0.8 eV lie basically on top of the line at -0.8 eV and are not shown. The experimental measurement is shown by the hatched area. (b) The reaction probability given by the $K_{^*\text{Si}^+}(T)/K_L$, Eqs. (18) and (20), for this reaction as a function of TS1 and TS2. The reaction probabilities for TS1 energies greater than 0 eV are ~ 0 ; for energies less than -0.8 eV, the curves lie essentially on top of the curve at -0.8 eV. The experimentally determined reaction probability is depicted by the shaded area. The values of TS1 and TS2 which are also calculated from the experimental measurement for the isotopic exchange fraction in (a) are given by the hatched area. It can be seen that there is a very narrow range of values for TS1 and TS2 which are consistent with both the reaction probability and the isotopic exchange fraction.

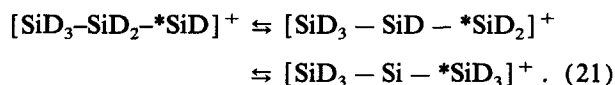
fraction nor the reaction probability alone are sufficient to fix a narrow range for the values of TS1 or TS2. The measurements combined, however, sharply delimit these two barrier energies. This can be seen by transposing the TS1/TS2 pairs which fit the experimentally measured exchange fraction from Fig. 5(a) onto Fig. 5(b) as shown. Values which are consistent with experiment are TS1 = -0.34 ± 0.05 eV and TS2 = -0.29 ± 0.04 eV.

Including the flux through TS3 explicitly [Eq. (A11)] changes the PST calculated values of TS1 and TS2 by less than 0.05% when the energy of TS3 is set equal to the *ab initio* calculated energy of -0.95 eV (Fig. 4).¹¹

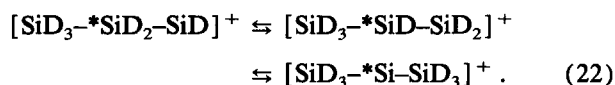
B. Si₂D₂⁺ + SiD₄

The microscopic steps of the second clustering reaction of Si₂D₂⁺ with SiD₄ are shown in Fig. 6. The reaction proceeds through an initial D-bridged complex, [D₂Si-Si⁺ ··· (SiD₄)], C1, similar to the first clustering step of Si⁺ with SiD₄. The next event involves a concerted insertion into a Si-D bond of SiD₄ by the two silicon centers of Si₂D₂⁺. This four center transition state is a fundamental departure from the three center Si-D insertion transition state of the Si⁺ reaction with SiD₄. *Ab initio* calculations do not find an equivalent three center transition state for the reaction of Si₂D₂⁺ with SiD₄.¹¹

The Si-D insertion leads to formation of the intermediate complex, [SiD₃-SiD₂-SiD]⁺, C2. Two 1,2 hydrogen shifts are quite energetically accessible from C2 which allows for isotopic scrambling of a labeled terminal silicon center,



However, if the label resides at the central silicon atom, that silicon center never becomes equivalent to one which originates from the original SiD₄, and no isotopic scrambling can occur;



From the Eqs. (21) and (22), it can be seen that the distribution of the silicon-29 label in the products depends on the relative amounts of the possible positions of this label in the C2 complex. The position of the label in C2 is given by the position of the label in the initial reactant, which in turn results from the previous reaction of ^{*}Si⁺ with SiD₄. In the reaction of ^{*}Si⁺ with SiD₄, rapid isotopic scrambling is found to occur via the [SiD₂-SiD₂] intermediate complex, which is denoted as C3 in Fig. 4. The final product, ^{*}Si₂D₂⁺, presumably contains a 50-50 mix of the two possible isotopically labeled species, [D₂Si-^{*}Si⁺] and [D₂^{*}Si-Si⁺]. Of these two reactants, only the former can undergo isotopic exchange. This can be seen from Eq. (21) and Fig. 6 where [D₂Si-^{*}Si⁺] forms an intermediate, C2, with the isotopic label residing on a terminal silicon atom as required in C4 for exchange. Since the other labeled reactant, [D₂^{*}Si-Si⁺], cannot undergo exchange, formation of unlabeled Si₂D₂⁺, Eq. (4), reflects just half of the total processes involving an

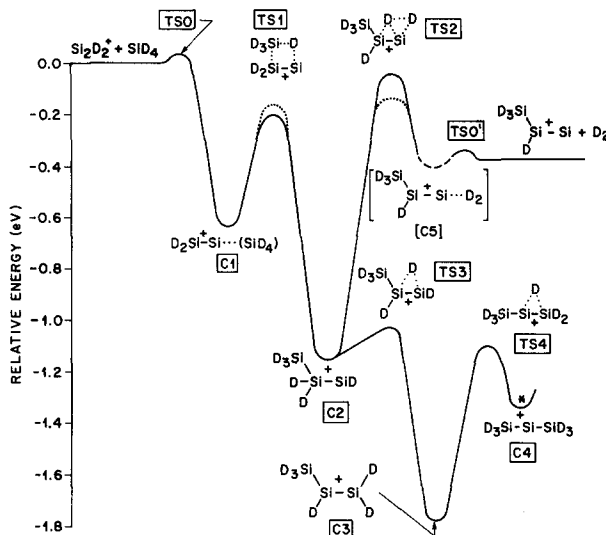


FIG. 6. Schematic potential energy surface depicting the important intermediates, C(1-5) and transition states, TS(0-4), for the reaction of Si₂D₂⁺ with SiD₄. The structure, C4, where scrambling of the silicon-29 isotope can occur for certain positions of the label, is designated by an asterisk [see Sec. IV B and Eqs. (21) and (22)]. Energies of the reactants, products, C(*i*) and T(*i*) are obtained from the calculations in Ref. 11 and are indicated by solid lines. The orbiting transition states at TS0 and TS0' are shown by solid lines through the average energy of these states at 300 K. The dashed line and brackets around the structure at [C5] are used to indicate that this structure and its energy have been estimated. Dotted lines at TS1 and TS2 give the energies calculated from the PST model which are consistent with experiment. Zero-point energies are included for all species; all energies are relative to the reactants which are set at zero energy. A true potential energy contour is not implied by the shape of the lines connecting the various energies along this surface.

overall back reaction. Furthermore, [D₂Si - ^{*}Si⁺] forms two isotopically labeled products, [^{*}SiD₃ - SiD-Si⁺] and [SiD₃-SiD-^{*}Si⁺]. The third possible isotopically labeled product, [SiD₃-^{*}SiD-Si⁺], is formed exclusively as the only product of the reactant [D₂^{*}Si-Si⁺].

The reaction dynamics along the potential surface in Fig. 6 are calculated using the PST theoretical model described for the reaction of Si⁺ with SiD₄. Similar assumptions pertain to the inclusion of important transition states and the treatment of the isotopic exchange processes. The expressions for the branching ratio I_E/I_R of isotopic exchange [Eq. (4)] relative to formation of ^{*}Si₃D₄⁺ [Eq. (3)], and the overall reaction probability, $K_{*Si_2D_2^+}(T)$ are almost the same as for ^{*}Si⁺ + SiD₄. The one difference is that only half of the labeled ^{*}Si₂D₂⁺ reactants can undergo isotopic scrambling. Therefore the observed branching ratio and overall reaction probability for ^{*}Si₂D₂⁺ are given by

$$\frac{I_E}{I_R} = \frac{\frac{1}{2}\omega_2(T)}{\omega_1(T)}, \quad (23)$$

$$K_{*Si_2D_2^+}(T) = \frac{F_0(T)[\omega_1(T) + \frac{1}{2}\omega_2(T)]}{\rho_R}. \quad (24)$$

The expressions for $\omega_i(T)$, $F_0(T)$, and $\rho_r(K_L)$ are evaluated as given in the Appendix using molecular constants appropriate to ^{*}Si₂D₂⁺ and the various reaction transition states shown in Fig. 6.

The results of the PST calculations of the isotopic exchange fraction, $[I_E/(I_E + I_R)]$ and reaction probability

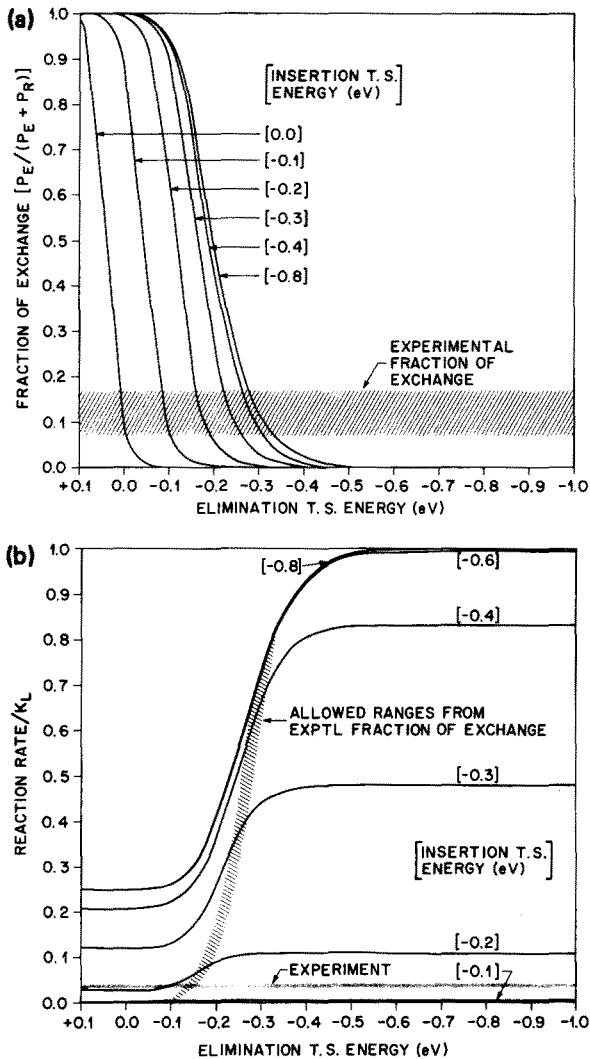


FIG. 7. PST calculations for the reaction of Si_2D_2^+ with SiD_4 , Eqs. (3) and (4), over a range of values for the insertion and elimination transition state energies (TS1 and TS2, Fig. 6). (a) The product fraction of isotopic exchange, per Eq. (23), as a function of TS1 and TS2. The curves for energies of TS1 which are less than -0.8 eV lie nearly on top of that curve. The experimentally measured isotopic exchange fraction is given for comparison by the hatched area. (b) The reaction probability $K_{\text{Si}_2\text{D}_2^+}(T)/K_L$, Eqs. (20) and (24), as a function of TS1 and TS2. Probabilities for the TS1 greater than -0.1 eV are essentially zero; the curves for the probabilities for TS1 less than -0.8 eV lie nearly on top of the curve at -0.8 eV. The probability obtained from experiment is given by the shaded area. Values of TS1 and TS2 which were calculated from the experimental measurement for the isotopic exchange fraction in (a) are given by the hatched area. The experimental measurements of the reaction probability and isotopic exchange fraction in concert determine a narrow range of values for TS1 and TS2 as shown in the hatched region.

$K_{\text{Si}_2\text{D}_2^+}(T)$ are given in Figs. 7(a) and 7(b) over a range of values for TS1 and TS2 in Fig. 6. As for the $\text{Si}^+ + \text{SiD}_4$ reaction, the overall reaction probability $K_{\text{Si}_2\text{D}_2^+}(T)$ is more dependent on the height of the insertion transition state activation barrier and the fraction of isotopic exchange is more dependent on the height of the elimination transition state barrier. When compared to the experimental determinations shown in Fig. 7(b), these quantities together determine the energies as $\text{TS1} = -0.16 \pm 0.02$ eV and $\text{TS2} = -0.14 \pm 0.02$ eV.

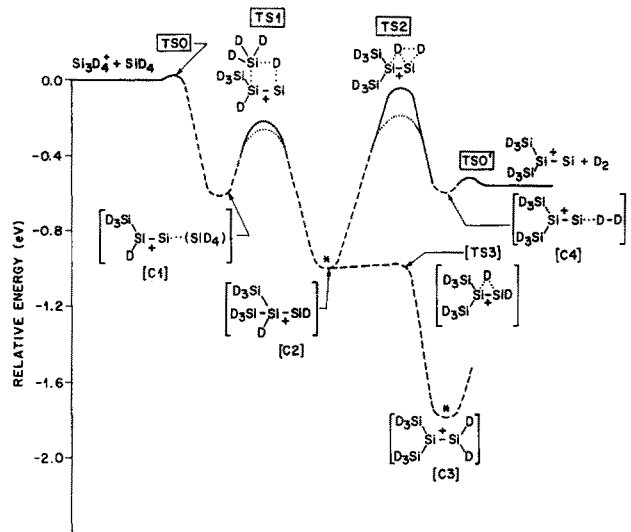
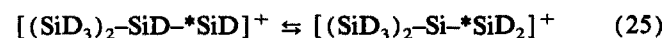


FIG. 8. The potential energy surface for the reaction of Si_3D_4^+ with SiD_4 , depicting the important intermediates, C(1–4) and transition states, TS(0–3). Scrambling of the silicon-29 isotope can occur in either C2 or C3 (which are starred) only if the label resides on one of the $-\text{SiD}_3$ groups [cf. Sec. IV C and Eqs. (25) and (26)]. Energies of the reactants, products, and T(i) indicated by solid lines are obtained from the calculations in Ref. 11 except for the orbiting transition states at TS0 and TS0' which are given by the average energy of these states at 300 K. The dashed lines and brackets around the structures at [C1–4] are used to indicate that these structures and energies have been estimated. Dotted lines at TS1 and TS2 give the energies calculated from the PST model which are consistent with experiment. Zero-point energies are included for all species; energies are relative to the reactants which are set at zero. A true potential energy contour is not implied by the shape of the lines connecting the various energies along this surface.

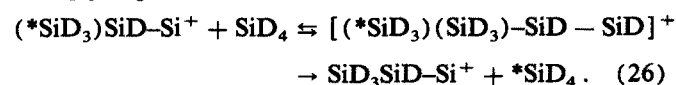
C. $\text{Si}_3\text{D}_4^+ + \text{SiD}_4$

The potential surface for the third clustering reaction in the sequence $\text{Si}_3\text{D}_4^+ + \text{SiD}_4$ is shown in Fig. 8. The microscopic steps leading to the formation of the product Si_4D_6^+ are completely analogous to the previous clustering reaction between Si_2D_2^+ with SiD_4 . The transition states TS1, TS2, and TS3 have nearly the same energies and geometries for both clustering reactions. This is not surprising since the main difference is a $-\text{SiD}_3$ substitution for a $-\text{D}$ in the corresponding structures.

The one contrast between the clustering reaction of Si_3D_4^+ and the previous one involving Si_2D_2^+ is the means by which isotopic exchange occurs. For the Si_2D_2^+ reaction, this is accomplished by two 1,2 hydrogen shifts which lead to a symmetric intermediate, C4, in Fig. 6. For Si_3D_4^+ , only one 1,2 hydrogen shift can occur, e.g.,



forming an intermediate [C3] where further migration of the deuteriums incorporated in the $-\text{SiD}_3$ groups is energetically unfeasible. The only possible isotopic exchange that can occur, then, is for a starting structure with a labeled $-\text{SiD}_3$ group;



From isotopic scrambling in the previous clustering step, the starting $^*Si_3D_4^+$ ion population consists of three isotopically labeled isomers, [$^*SiD_3-SiD-Si^+$], [$SiD_3-^*SiD-Si^+$], and [$SiD_3-SiD-^*Si^+$] in the ratio of 1:2:1. Only the first structure can undergo the exchange process described by Eq. (26). Consequently, the observed isotopic exchange reaction Eq. (6) represents only a quarter of the total back reactions and the respective position of the original isotopic label in the three structures given above are retained in the $^*Si_4D_6^+$ product.

The phase space model calculations are performed as described previously for $Si_2D_2^+$ and Si^+ reactions with SiD_4 . The limitations on the available isotopic exchange process are accounted for in the expressions for the isotope branching ratio I_E/I_R and overall reaction probability $K_{^*Si_3D_4^+}(T)$;

$$\frac{I_E}{I_R} = \frac{\frac{1}{4}\omega_2(T)}{\omega_1(T)}, \quad (27)$$

$$K_{^*Si_3D_4^+}(T) = \frac{F_0(T)[\omega_1(T) + \frac{1}{4}\omega_2(T)]}{\rho_R}, \quad (28)$$

$\omega_i(T)$, $F_0(T)$, and $\rho_R(K_L)$ are computed as described in the Appendix using molecular constants calculated by Raghavachari for $^*Si_3D_4^+$ and the transition states appropriate to its reaction with SiD_4 , Fig. 8.¹¹

The results of the PST calculations are summarized in Figs. 9(a) and 9(b) for the isotopic exchange fraction [$I_E/(I_E + I_R)$], and the reaction probability $K_{^*Si_3D_4^+}(T)$ as a function of TS1 and TS2. As for the previous two cluster reactions, $K_{^*Si_3D_4^+}(T)$ is more affected by the height of the insertion transition state barrier, TS1, whereas [$I_E/(I_E + I_R)$] is more affected by the height of the elimination transition state barrier, TS2. Values of these barrier heights which are mutually consistent with experiment, Fig. 9(b), are $TS1 = -0.27 \pm 0.02$ eV and $TS2 = -0.19 \pm 0.02$ eV.

$Si_4D_6^+ + SiD_4$

The final clustering step observed during the time scale of our experiments is the bimolecular attachment of SiD_4 to $Si_4D_6^+$, forming $Si_5D_{10}^+$.²¹ A striking aspect of the reaction of $Si_4D_6^+$ is that addition of $-SiD_2$ accompanied by loss of D_2 is no longer observed. The reason for this can be seen in the microscopic reaction pathway described by Fig. 10.¹¹ As for the three previous clustering steps, the reaction begins with formation of an initial deuterium bridged complex, [$(SiD_3)_2Si_2^+ \cdots (SiD_4)$], [C1] followed by a concerted four center insertion into a Si-D bond of SiD_4 at TS1. The resulting [$Si_5D_{10}^+$] reaction intermediate, C2, however, contains only one labile deuterium with the remaining deuteriums incorporated in stable $-SiD_3$ groups. In this highly branched structure, any deuterium migration which might lead to an elimination type of transition state is energetically disallowed.¹¹ Loss of either a D atom or a $\cdot SiD_3$ radical from the C2 [$Si_5D_{10}^+$] complex is also quite endothermic.²⁹ So, the only possible exothermic reaction of $Si_4D_6^+$ is formation and stabilization of the intermediate C2 [$Si_5D_{10}^+$] complex itself. This can occur either by radiative energy loss or collisional stabilization.

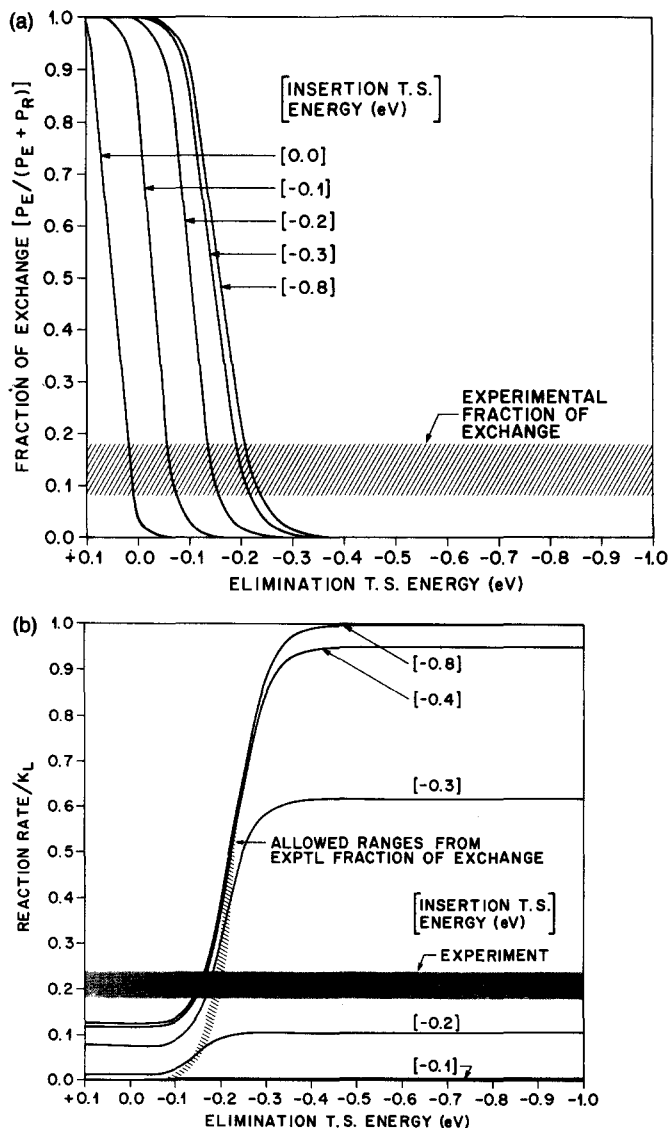
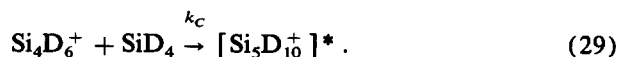


FIG. 9. PST model calculations for the reaction of $Si_3D_4^+$ with SiD_4 , Eqs. (5) and (6), plotted for a range of values of the insertion and elimination transition state energies (TS1 and TS2 in Fig. 8). (a) The fraction of isotopic exchange, derived from Eq. (27), relative to the total products as a function of the energies of TS1 and TS2. The experimentally measured isotopic exchange fraction is given by the hatched area. The curves for values of the insertion transition state energy which are less than -0.8 eV lie essentially on top of the curve for -0.8 eV and are not shown. (b) The reaction probability, $K_{^*Si_3D_4^+}(T)/K_L$, Eqs. (20) and (28), as a function of the energies of TS1 and TS2. For energies greater than -0.1 eV, the reaction probability is ~ 0 ; the curves for energies less than -0.8 eV lie nearly on top of the curve at -0.8 eV. The experimental value for the probability is given in the shaded area and the TS1/TS2 values which are determined from the experimental value for the isotopic exchange fraction in (a) lie in the hatched area. Only a very narrow range of values for TS1 and TS2 are mutually consistent with experiment.

The probability for the process of forming and quenching the [$Si_5D_{10}^+$] complex is also calculated using the PST model with the following kinetics mechanism. The energized [$Si_5D_{10}^+$] complex is formed in a collision of $Si_4D_6^+$ with SiD_4 ,



[$Si_5D_{10}^+$] * decays unimolecularly,

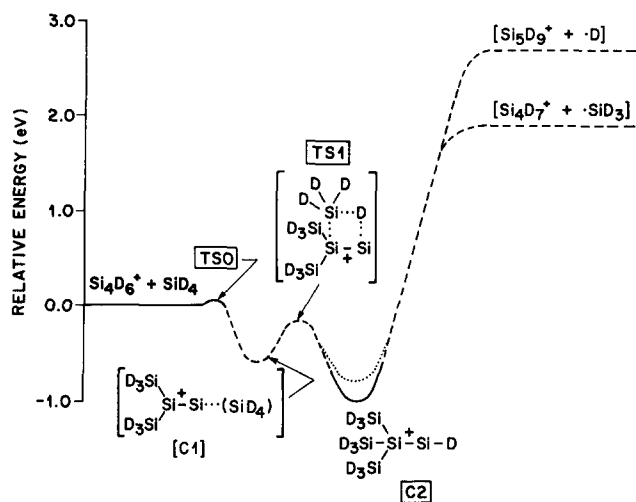


FIG. 10. Potential energy surface for the reaction of Si₄D₆⁺ with SiD₄ indicating the important intermediates, C(1–2), and transition states TS(0–1). The reaction proceeds through a pathway similar to the first three clustering reactions involving Si–D insertion (TS1). The insertion complex, C2, however, contains only one unsaturated silicon center such that access is blocked to a D₂ elimination transition state similar to TS2 for the previous clustering reactions. The only exothermic product of this reaction is the stabilized Si₅D₁₀⁺ intermediate complex. The *ab initio* calculated energy for this complex is given by the solid line; the dotted line shows the energy calculated using the PST model to determine the rate of formation of Si₅D₁₀⁺ at the pressures used in these experiments. Dashed lines and brackets around the structures at C1 and TS1 are used since these complex structures and energetics are estimated from the previous clustering step of *Si₃D₄⁺ with SiD₄. Two possible products are also shown, loss of a deuterium atom and loss of a –SiD₃ radical. The estimated energetics of these two channels, given by the dashed lines, are highly approximate since they are derived from Si–H and Si–SiH₃ bond energies for stable silane species (Ref. 29). Zero-point energies are included for all species; energies are all relative to the Si₄D₆⁺/SiD₄ reactants which are set at zero energy. A true potential energy surface contour is not intended by the shape of the interconnecting lines between the various TSi and Ci.



unless stabilization of this complex occurs, which will be essentially by collisions with a third body. In our experiments, the third body quencher will be another SiD₄ molecule,



A factor of β , which can have values from 0–1.0, is introduced into the Langevin collision rate in Eq. (31) since not every collision is expected to remove sufficient energy to stabilize the [Si₅D₁₀⁺]^{*} complex. The concentration of [Si₅D₁₀⁺]^{*} is derived using a steady state approximation for the time dependence of [Si₅D₁₀⁺]^{*};

$$[\text{Si}_5\text{D}_{10}^+]^* = \frac{k_C [\text{Si}_4\text{D}_6^+] [\text{SiD}_4]}{k_D + \beta K_L [\text{SiD}_4]}. \quad (32)$$

The decay of Si₄D₆⁺ is described by

$$\frac{d[\text{Si}_4\text{D}_6^+]}{dt} = -k_C [\text{Si}_4\text{D}_6^+] [\text{SiD}_4] \left(\frac{\beta K_L [\text{SiD}_4]}{k_D + \beta K_L [\text{SiD}_4]} \right), \quad (33)$$

$$\frac{[\text{Si}_4\text{D}_6^+]}{[\text{Si}_4\text{D}_6^+]_0} = e^{-\kappa t}, \quad (34)$$

$$\kappa = k_C [\text{SiD}_4] \left(\frac{\beta K_L [\text{SiD}_4]}{k_D + \beta K_L [\text{SiD}_4]} \right). \quad (35)$$

Assuming that every collision between Si₄D₆⁺ and SiD₄ leads to formation of the [Si₅D₁₀⁺]^{*} complex, k_C is given by the Langevin rate, $K_L = 9.22 \times 10^{-10} \text{ cm}^3 \text{ molecule}^{-1} \text{ s}^{-1}$ for Si₄D₆⁺/SiD₄ collisions [Eq. (20)]. The experimental measurement for $\kappa/[\text{SiD}_4]$ at a pressure of 2.0×10^{-7} Torr is

$$\begin{aligned} \kappa/[\text{SiD}_4] &= 1.0 \pm 0.3 \times 10^{-13} \text{ cm}^3 \text{ molecule}^{-1} \text{ s}^{-1} \\ &= 9.22 \times 10^{-10} \left(\frac{5.9\beta}{k_D + 5.9\beta} \right) \text{ cm}^3 \text{ molecule}^{-1} \text{ s}^{-1}. \end{aligned} \quad (36)$$

The factor $[5.9\beta/(k_D + 5.9\beta)]$ is calculated from a PST model for k_D . The microscopic rate $k_D(E, J)$ for the dissociation of [Si₅D₁₀⁺]^{*}, with an initial energy E and angular momentum J , is given by

$$k_D(E, J) = \frac{F_0(E, J)}{h 2J\rho_{[\text{Si}_5\text{D}_{10}^+]^*}(E_{\text{vib}})}, \quad (37)$$

where $\rho_{[\text{Si}_5\text{D}_{10}^+]^*}(E_{\text{vib}})$ is the density of vibrational states of the energized [Si₅D₁₀⁺]^{*} complex at the available vibrational energy E_{vib} . Further details for calculating $k_D(E, J)$, $F_0(E, J)$, and $\rho_{[\text{Si}_5\text{D}_{10}^+]^*}(E_{\text{vib}})$ are given in the Appendix. The experimental observable $\Omega(T)$ is determined by averaging over the Boltzmann distribution of energies of the reactants at $T = 300$ K and the allowed values of J ,

$$\begin{aligned} \Omega(T) &= \int_0^\infty dE e^{-E/kT} \int_0^{J_{\text{MAX}}} dJ 2JF_0(E, J) \\ &\quad \times \left(\frac{5.9\beta}{k_D(E, J) + 5.9\beta} \right) / \\ &\quad \int_0^\infty dE e^{-E/kT} \int_0^{J_{\text{MAX}}} dJ 2JF_0(E, J). \end{aligned} \quad (38)$$

The quenching efficiency factor β is assumed to be independent of temperature.

The values of $\Omega(T)$ over a range of energies assumed for the [Si₅D₁₀⁺]^{*} complex are plotted in Fig. 11 with and without including the internal rotations as described in the Appendix. As shown in Fig. 11, the effect of including internal rotation is to raise the phase space theoretical value for the energy of this complex by about 0.05 eV. Since Si₄D₆⁺ and the [Si₅D₁₀⁺]^{*} complex contain two and three internal –SiD₃ rotors, respectively, treatment of internal rotation is probably warranted. In addition, there is a large uncertainty in the derived values for the frequencies of the five torsional modes (which are converted to rotations).¹¹ These five modes are quite low in frequency and figure prominently in the density of states in our phase space calculations. Despite this, however, the calculated value for the complex is not

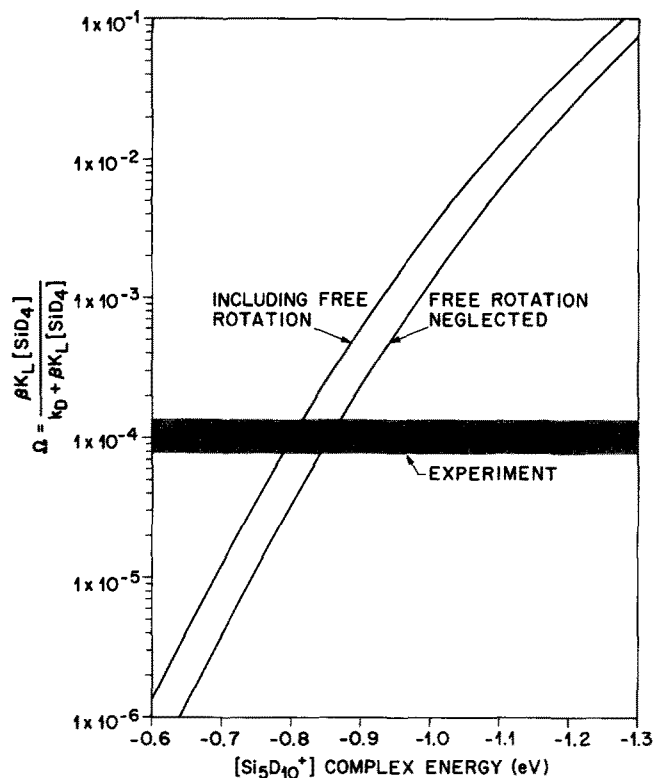


FIG. 11. PST model calculations for the association reaction of Si₄D₆⁺ with SiD₄, Eq. (7), over a range of energies for the [Si₅D₁₀⁺] complex (C2 in Fig. 10). The rate constant factor Ω describes the probability for collisional stabilization of the energized [Si₅D₁₀⁺] complex as a function of the [Si₅D₁₀⁺] complex energy, Eqs. (33)–(36). The results are given for calculations with and without explicit inclusion of free internal rotation in the determination of the density of states (see Sec. IV D). The calculations plotted here assume a collisional efficiency factor, β , of unity.

greatly sensitive to the absolute value of these torsional frequencies: raising or lowering the values of these frequencies by about 50% lowers or raises, respectively, the calculated energy of the [Si₅D₁₀⁺] complex by only 0.03 eV. Nonetheless, explicit treatment of these five torsions as free internal rotations ameliorates this uncertainty. For $\beta = 1.0$, and in-

cluding free internal rotation, the best fit to the experimentally derived value for $\Omega(T)$ ($1.1 - 0.3 \times 10^{-4}$) is obtained for a well depth of the [Si₅D₁₀⁺] complex of -0.80 ± 0.02 eV. As β decreases, the calculated well depth for the [Si₅D₁₀⁺] complex increases. Collision efficiency factors of $\beta = 0.50$ and 0.10 , for example, yield a [Si₅D₁₀⁺] complex energy of -0.84 and -0.92 eV, respectively. The *ab initio* calculation of this energy is -0.98 eV which can be obtained exactly only when $\beta = 0.02 - 0.03$. This is an unreasonably low efficiency factor for a quenching collision of [Si₅D₁₀⁺] by SiD₄ since there is a good match between some of their vibrational frequencies. For example, β is found to be near unity for [(N₂)₂⁺]-N₂ collisions.³⁰ By analogy, β should be nearly one for [Si₅D₁₀⁺]-SiD₄ collisions as well.

V. DISCUSSION

A. Comparison of theory and experiment

The fruitful interplay of phase space theory and the mechanistic electronic structure calculations of Raghavachari¹¹ yield details for each clustering reaction which are entirely consistent with our experimental findings. Qualitatively, the sequence of the clustering reactions involving only three stepwise additions of -SiD₂, followed by attachment of SiD₄, is accounted for. The isotopic exchange process is also accurately predicted. Quantitatively, the phase space theoretical calculations of the energetics along the reaction pathways in Figs. 4, 6, 8, and 10 coincide with the *ab initio* calculations. Table II shows the transition state and intermediate complex energies taken from the *ab initio* calculations of Raghavachari in comparison with those deduced from fitting the experimental data using phase space theory. In absolute terms, the activation energies generally agree to within 0.12 eV (3 kcal/mol) with the exception of the second elimination transition state, TS2, for the *Si⁺ + SiD₄ reaction.

In many cases, the activation energies derived from experiment/PST are slightly lower than those found in the *ab initio* calculations of Raghavachari. This is not surprising since *ab initio* electronic structure calculations tend to sys-

TABLE II. Comparison of PST and *ab initio* calculations of transition state (TS1–2) or intermediate complex (C2) energies for each sequential clustering reaction of ²⁹Si⁺ with SiD₄.^a

Reaction	Energy (eV)			<i>Ab initio</i> calculations		
	PST calculations	TS2	C2	TS1	TS2	C2
*Si ⁺ + SiD ₄ → { *Si ₂ D ₂ ⁺ + D ₂ / Si ⁺ + *SiD ₄	-0.34 ± 0.05	-0.29 ± 0.04	...	-0.46	-0.01	...
*Si ₂ D ₂ ⁺ + SiD ₄ → { *Si ₃ D ₄ ⁺ + D ₂ / Si ₂ D ₂ ⁺ + *SiD ₄	-0.16 ± 0.02	-0.14 ± 0.02	...	-0.21	-0.05	...
*Si ₃ D ₄ ⁺ + SiD ₄ → { *Si ₄ D ₆ ⁺ + D ₂ / Si ₃ D ₄ ⁺ + *SiD ₄	-0.27 ± 0.02	-0.19 ± 0.02	...	-0.21	-0.06	...
Si ₄ D ₆ ⁺ + SiD ₄ → Si ₅ D ₁₀ ⁺ ^b	-0.80 ± 0.02 ^c	-0.98

^aNotations for various transition states/complexes refer to Figs. 4, 6, 8, and 10. Zero-point energies are included in the energies listed.

^bOnly unlabeled Si₄D₆⁺ reactions were examined (Ref. 21).

^cThis value is for a PST calculation which includes free internal rotation and sets the collision efficiency factor β equal to unity (see Sec. IV D).

tematically underestimate bond strengths. This produces errors which cancel to some degree, since the calculated transition state energies are referenced to the calculated reactant energies. The reactants, however, all have fewer bonds than the transition states which produces a systematic overestimation of the energies of the transition states. Furthermore, the geometries in the electronic structure calculations have been optimized at the Hartree–Fock level. Additional geometry optimization at higher levels of calculation would lower the energy of the reactants but may either raise or lower the total energies of the transition states depending on the nature of the potential energy surface near the saddlepoint. This affects not only the calculations of the energies of the transition states but also the molecular constants which enter into the phase space theoretical calculations (see the Appendix). Similarly, the errors in determining the molecular constants will be partially ameliorated when referenced to reactant molecular constants although the best comparison is probably between transition states. For these reasons, these *ab initio* electronic structure calculations (and the phase space calculations as well) are expected to be most reliable for the relative energies of the two transition states, TS1 and TS2. In relative terms, the PST calculated energy differences between TS1 and TS2 agree, within error limits, to 0.10 eV (2 kcal/mol) for the reaction of Si₂D₂⁺—and to within 0.03 eV (1 kcal/mol) for the reaction of Si₃D₄⁺.

The binding energy of the Si₃D₁₀⁺ complex from both experiment/PST and *ab initio* theory can only be compared in absolute numbers which are also in reasonable agreement. The PST value is somewhat higher but represents an upper limit since unit collisional quenching efficiency is assumed in the calculations. These correspondences are probably as good as can be expected considering the approximations made in the phase space theoretical model, which include harmonic oscillations, spherical three-dimensional rotors, and a point charge ion induced dipole potential for the orbiting transition states.

The match between experiment/phase space calculations and Raghavachari's *ab initio* calculations of the second transition state energy, TS2, for the *Si⁺SiD₄ reaction is not as good as for the other reactions. The activation energy from *ab initio* theory for TS2 is 0.28 eV higher than the experimental/PST value; whereas for TS1 the activation energy from *ab initio* theory is 0.12 eV lower. While these discrepancies are minor, there clearly is not as good of an agreement for this reaction as for the others, for reasons which are not obvious. One possibility is that the *Si⁺ + SiD₄ system is sufficiently small that the statistical assumptions in the phase space transition state theoretical approach are beginning to break down and the dynamics of the reaction are becoming important. Dynamical considerations would rationalize the discrepancy at TS1 but do not provide a straightforward explanation as to why TS2 should be lower. On the other hand, the problem could be that the position of the lowest saddlepoint for TS2 has not been found in the *ab initio* calculations. Additional experiments measuring the translational energy release during the reaction or angular resolution of the products would shed further light on the details of the potential surface of this reaction but are obvi-

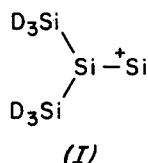
ously beyond the scope of the techniques used in our work.

Recent ion-beam experiments by Boo and Armentrout have examined the reaction products of Si⁺ with SiD₄/SiH₄ as a function of collision energy.²³ These studies confirm earlier ion cyclotron resonance experiments by Henis *et al.*, which showed that Si₂D₂⁺/Si₂H₂⁺ are exothermic products.²² The ion-beam experiments also uncovered the isotopic exchange process for reactions of Si⁺ with both SiD₄ and SiH₄ at low collision energies. The isotopic exchange cross section, however, was found to increase at low kinetic energies to a maximum at about 0.1 eV and then decrease at higher energies. From this data, the isotopic exchange process was interpreted to be overall endothermic by 0.03–0.12 eV. Our experiments show that isotopic exchange is *exothermic* at room temperature where the average energy is 0.03 eV. Under all pressure conditions, we observe that isotopic exchange and Si₂D₂⁺ formation track each other in time and relative intensity. This is only consistent with a potential surface such as Fig. 4 where isotopic exchange does not require a separate endothermic mechanism. Boo and Armentrout propose several possible mechanisms for these processes, of which one matches the overall pathway of Fig. 4. In all of the mechanisms that have been suggested in the ion-beam work, isotopic exchange and Si₂(D/H)₂⁺ product formation occur along a mutually consistent pathway. The only way that these mechanisms could cause the isotopic exchange process to be endothermic would be for one or more of the requisite hydrogen/deuterium migration steps to be endothermic. The *ab initio* calculations show clearly that these migrations are energetically quite feasible. A closer examination of the ion-beam data indicates that they appear to be consistent with our results. The reaction rate constant calculated from the ion-beam cross sections for Si₂D₂⁺ formation is $8 \pm 2 \times 10^{-10}$ cm³ molecule⁻¹ s⁻¹, which is in excellent accord with our results (Table I).³¹ At energies of ~0.1 eV, the isotope exchange process represents 5%–13% of the total products which agrees with our measured product branching ratio, Table I. The decreases in the measured isotopic exchange cross sections at lower energies may occur for different reasons. In the ion beam experiments, the reactions are driven with kinetic energy. The reaction potential surface calculated by Raghavachari for this reaction (Fig. 4) involves a complex pathway with multiple transition states. The reaction cross sections for a complicated surface may not exhibit a simple monotonic decrease with increasing kinetic energy. For example, vibrational energy may be more effective than translational energy for driving the isotope exchange process. If translational and internal energy are not totally equilibrated during the reaction, then it may well be that the isotopic exchange cross section would temporarily decrease with increasing collision energy. This possibility could be examined in more detail using phase space theoretical calculations which treat vibrational, rotational, and translational energies separately or using trajectory type calculations to explore the rate across the total potential energy surface. The Boo and Armentrout data also show a dramatic falloff of nearly an order of magnitude in the isotopic exchange cross sections as the kinetic energy approaches zero for ²⁹Si⁺ and ³⁰Si⁺ as compared to ²⁸Si⁺ which falls off only

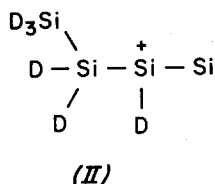
by about 25%. This may be an indication that at very low energies, the Si⁺ ions are trapped in the collision cell for longer times. The additional time spent in the collision cell may also be sufficiently long to allow for the isotopically scrambled product to react further with SiD₄/SiH₄ to form the favored Si₂D₂⁺/Si₂H₂⁺ product or exchange back to the most abundant ²⁸Si⁺ isotope. These additional reactions would lead to an apparent loss of isotopically exchanged ²⁹Si⁺ and ³⁰Si⁺ but have less of an effect on the ²⁸Si⁺ which would still continue to be regenerated during additional isotopic exchange.

B. Implications for prenucleation of hydrogenated silicon particles

Sequential clustering with SiD₄, starting with Si⁺, clearly does not provide a means for rapid formation of the requisite nuclei for spontaneous growth of hydrogenated silicon dust. The promise of infinite polymerization is suggested by three initial clustering reactions. These, however, result in a branched hydrogenated silicon species, e.g., the Si₄D₆⁺ structure shown in (I);



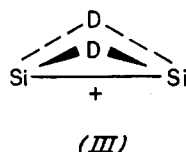
instead of a linear polymer, e.g., the Si₄D₆⁺ structure shown in (II);



where growth can continue *ad infinitum* at the terminal unsaturated silicon. Energetically, the linear polymer isomers should be quite feasible. The reason that they are not formed is because that would require the silane insertion reaction to proceed through endothermic intermediates.¹¹

The constraints of the silane reaction mechanism also limit reaction of Si₅D₁₀⁺ even though it still contains an unsaturated silicon center. This suggests that electron counting schemes and similar devices will give erroneous predictions for these reactions. Eighteen electron and topological electron counting "rules" have been devised to describe the packing and electron deficiency of coordinated metal clusters.³²⁻³⁴ They have been used with some degree of success in accounting for rates and products observed in gas phase clustering of transition metal ion carbonyls.⁷⁻¹⁰ The basic tenet of these approaches, however, is that there is continual rearrangement of the growing transition metal cluster to form the most stable metal-ligand bonded structure. An obvious corollary of these counting rules is that the reaction mechanism must be inconsequential or of secondary importance. We have shown that in the clustering reactions of Si⁺ with SiD₄, the reaction mechanisms are of the utmost importance in determining the product cluster structures and there

is little or no rearrangement to form the most stable product isomer. For example, D₂Si-Si⁺, which is formed in the reaction of Si⁺ with SiD₄, is not the most stable isomer. Another structure (III)



where both deuteriums are bridging between the silicon atoms is favored by ~0.3 eV.¹¹ The latter most stable isomer is not formed in the Si⁺ + SiD₄ reaction, however, because that would require traversing a D₂ elimination transition state which is calculated to be 0.4 eV endothermic.¹¹

Finally, the clustering reaction sequence of Si⁺ with SiD₄ provides an excellent illustration of how minor energetic differences during a reaction can lead to major differences in reaction rate. The reaction mechanism is basically the same for all three clustering reactions. Corresponding transition states only differ in energy by ~0.2 eV (5 kcal/mol). Yet, the reaction probability oscillates by factors of 10-20. The large changes in reaction probability for these three reactions arise both because of the small energy differences among the transition states and the increase in the density of states with increased molecular size which affects the microscopic fluxes through the various transition states (see Figs. 5, 7, 9, and 11). This suggests that large errors can result when the reaction rates for a presumed reaction sequence are assumed to be essentially equal to the reaction rate of the first step.

The sequential clustering reactions of Si⁺ with SiD₄ do not lead to the exothermic formation of large cluster particles. Of course, a multitude of other precursors exist in the silane plasma primordial soup including neutral pyrolytic fragments such as silicon atoms and SiH₂.⁴ The particulate formation model developed by Kushner emphasizes the role of these neutral fragments in the growth of large particles.⁵ The neutral clustering reactions need not necessarily mimic the ionic clustering reactions and comparisons should be made with caution. Nonetheless, we hope that detailed information of this type will contribute to the understanding of heterogeneous nucleation and assist the daunting task of building believable cluster growth models.

VI. CONCLUSIONS

The reaction rates and products of the sequential clustering reactions of ²⁹Si⁺ with SiD₄ are observed, starting with ground state ²⁹Si⁺ and terminating with Si₅D₁₀⁺ on the time scale of these experiments. The first three clustering reactions proceed by stepwise addition of -SiD₂ and loss of D₂. In all of these reactions, isotopic exchange of the labeled silicon-29 with SiD₄ competes with addition of -SiD₂. Following formation of Si₄D₆⁺, this clustering reaction suddenly ceases and further cluster growth occurs only by attachment of SiD₄.

The observed clustering sequence and isotopic exchange are consistent with the mechanisms for the individual clustering steps which have been determined by Raghavachari

using *ab initio* electronic structure calculations. These calculations also show that the Si_{*n*+1}D_{2*n*}⁺ products have structures which are highly branched. Ultimately, this leads to a cluster, Si₄D₆⁺, which can add SiD₄ but not eliminate D₂.

The experimental results have been used in concert with the potential surfaces determined by Raghavachari to calculate the transition state barriers in the first three clustering reactions using statistical phase space transition state theory. Since both the forward and reverse (isotope exchange) reaction probabilities are measured, the energetics of both the initial Si–D insertion transition state and the final D₂ elimination transition state can be derived from the phase space model. Reasonable agreement, within 0.28 eV, with the *ab initio* calculations for these two transition state energies is found for the first reaction of ²⁹Si⁺ + SiD₄. The inter-consistency between the phase space theory and *ab initio* results is particularly good for the next two reactions of ²⁹Si₂D₂⁺ and ²⁹Si₃D₄⁺ with SiD₄, the largest discrepancy being less than 0.12 eV. Phase space theory is also used to model the binding energy of the Si₅D₁₀⁺ association complex and yields an energy which is within 0.2 eV of the *ab initio* value.

The sequential clustering of Si⁺ with SiD₄ thus encounters an early bottleneck which prevents rapid formation of a critical nucleus required for spontaneous growth of large hydrogenated silicon particles. This limitation is not expected based on a simple extrapolation of the reaction of Si⁺ with SiD₄, nor is it rationalized by the degree of saturation in the terminal Si₄D₆⁺ product. Similar bottlenecks may well exist in other reaction systems and determine the prerequisites for prenucleation of particulates.

ACKNOWLEDGMENT

We would like to thank Professor P. Armentrout for discussions regarding his ion-beam results.

APPENDIX

1. Derivation of various reaction probabilities (ω_i) for reactions (1) and (2)

The isotopic exchange and reaction probabilities for the reaction of *Si⁺ + SiD₄ are derived from the potential surface in Fig. 4. In the following discussion, *P* denotes a probability for an individual microscopic process, *F_i* denotes a flux through a given transition state TS*i* (e.g., *F₀* is the flux through the orbiting transition state, TS0 in Fig. 4), *n* is the number of times a particular trajectory is repeated, and the notation for the various transition states, intermediate complexes, etc., references Fig. 4.

An analysis of the potential surface in Fig. 4 indicates that the probability of product (*Si₂D₂⁺ + D₂) formation, $\omega_1(E, J)$, for a given *E* and *J*, is¹³

$$\omega_1(E, J) = \sum_{n=0}^{\infty} P^{n+1}(C1 \rightarrow C2) \times P^n(C2 \rightarrow C1)P(C2 \rightarrow \text{Products}), \quad (\text{A1})$$

$$P(C1 \rightarrow C2) = \frac{F_1}{F_1 + F_0}, \quad (\text{A2})$$

$$P(C2 \rightarrow C1) = \frac{F_1}{F_1 + F_2}, \quad (\text{A3})$$

$$P(C2 \rightarrow \text{Products}) = \frac{F_2}{F_1 + F_2}. \quad (\text{A4})$$

Note that the expression for $\omega_1(E, J)$ does not include the orbiting transition state, TS0', in the product channel. This is justified because the centrifugal barrier in the exit channel is small relative to the exothermicity of the reaction. Also, processes accessing TS3 and C3 are omitted since these lie at energies well below the other transition states (see below). Performing the summation over *n* in Eq. (A1) gives the following expression for $\omega_1(E, J)$ in terms of the fluxes,

$$\omega_1(E, J) = \frac{F_2}{F_0 + F_2 + F_2F_0/F_1}. \quad (\text{A5})$$

Similarly, the probability for isotopic exchange, $\omega_2(E, J)$, is 1/2 of the probability of accessing the intermediate, C2 without continuing on to form products,

$$\omega_2(E, J) = \frac{1}{2} \sum_{n=0}^{\infty} P(C1 \rightarrow C2)P^n(C1 \rightarrow C2) \times P^{n+1}(C2 \rightarrow C1)P(C1 \rightarrow \text{Reactants}). \quad (\text{A6})$$

This expression reduces to

$$\omega_2(E, J) = \frac{1}{2} \frac{F_0F_1F_1}{(F_0 + F_1)(F_0F_2 + F_1F_2 + F_0F_1)}. \quad (\text{A7})$$

The fluxes $\omega_i(E, J)$ for the various processes are given by the sum of states of the transition state complex with an energy *E* relative to the height of the activation barrier *E_i*. The total orbiting transition state flux *F₀* is

$$F_0(E, J) = \frac{1}{h} \int_0^{E-E_0} \rho_v(E - E_0 - E_{tr}) \times \Gamma_{ro}(E_{tr}, J) dE_{tr}, \quad (\text{A8})$$

where Γ_{ro} is the sum of rotational–orbital states at the rotational–translational energy, *E_{tr}*, and $\rho_v(E - E_0 - E_{tr})$ is the density of vibrational states of the *Si⁺–SiD₄ orbiting pair at the vibrational energy (*E - E₀ - E_{tr}*); *E₀* is the energy of the separated reactant pair. For the orbiting state of *Si⁺ + SiD₄, the rotational density of states is calculated assuming a sphere–atom collision pair.¹³ The total flux *F_i* at each of the tightly bound transition states, e.g., TS1 and TS2, is given by

$$F_i(E, J) = [N_i^V(E - E_i - B_i^S J^2)2J/h], \quad (\text{A9})$$

where $N_i^V(E - E_i - B_i^S J^2)$ is the sum of vibrational states of the transition state complex at TS*i* with vibrational energy less than or equal to (*E - E_i - B_i^SJ²*). *E_i* is the energy of the activation barrier at TS*i* and *B_i^S* is the rotational constant of TS*i* using a spherical top approximation,

$$B_i^S = (A_i B_i C_i)^{1/3}. \quad (\text{A10})$$

The molecular constants used to calculate the transition state fluxes for the *Si⁺ + SiD₄ reaction are obtained from quantities calculated for the corresponding Si/H species by Raghavachari.¹¹ Both vibrational frequencies and rotational

constants are corrected for the isotope effect, assuming that the intramolecular distances do not change upon deuteration.³⁵ Vibrational frequencies are also corrected for the systematic overestimation which is well known for Hartree–Fock derived force constants. The rotational constants are summarized in Table III.³⁶

The expressions for $\omega_i(E, J)$ can be modified to explicitly include the isotopic exchange process involving TS3 and C3. This adds an additional factor to the expression for $\omega_2(E, J)$,

$$\omega_2(E, J) = \frac{1}{2} \left[\frac{F_0 F_1 F_1}{(F_0 + F_1)(F_0 F_2 + F_1 F_2 + F_0 F_1)} \right] \times \left[\frac{F_3}{F_0 F_1 / (F_0 + F_1) + F_2 + F_3} \right]. \quad (\text{A11})$$

For large fluxes through TS3 relative to the other transition states, F_{0-2} , this equation for $\omega_2(E, J)$ reduces to the previous expression in Eq. (A7). The equation for $\omega_1(E, J)$ does not change.

2. Derivation of various reaction probabilities (ω_i) for reactions (3)–(6)

The isotopic exchange and reaction probabilities for the reactions of $^*\text{Si}_2\text{D}_2^+$ and $^*\text{Si}_3\text{D}_4^+$ with SiD_4 , Figs. 6 and 8, respectively, are obtained as described above for $^*\text{Si}^+$. The expressions in Eqs. (A5) and (A7) for $\omega_i(E, J)$ are the same with the $F_i(E, J)$ of the tightly bound transition states evaluated according to Eqs. (A9) and (A10) using appropriate molecular constants corrected for deuteration; see Table III.¹¹ In order to evaluate the orbiting transition state

TABLE III. Reactant, transition state, and intermediate complex molecular rotational constants used in the phase space calculations.^a

Species	Rotational constants (cm ⁻¹)		
	A	B	C
SiD ₄ ^b		1.483	
TS1 (Si ₂ D ₄ ⁺) ^c	1.119	0.136	0.133
TS2 (Si ₂ D ₄ ⁺) ^c	1.153	0.181	0.163
Si ₂ D ₂ ⁺	2.724	0.183	0.172
TS1 (Si ₃ D ₆ ⁺)	0.158	0.087	0.061
TS2 (Si ₃ D ₆ ⁺)	0.176	0.054	0.047
Si ₃ D ₄ ⁺	0.428	0.056	0.051
TS1 (Si ₄ D ₈ ⁺)	0.114	0.036	0.030
TS2 (Si ₄ D ₈ ⁺)	0.062	0.056	0.031
Si ₄ D ₆ ⁺	0.063	0.051	0.029
C2 (Si ₅ D ₁₀ ⁺)	0.032	0.031	0.027

^a Rotational constants obtained using geometry calculations of Raghavachari (Ref. 11). Note that his calculations are for hydrogenated species, whereas these experiments were performed on the corresponding deuterated species. In calculating the rotational constants reported in this table, it has been assumed that the geometries are the same for both the hydrogen and deuterium species except where otherwise noted.

^b Obtained from the rotational constant for SiH₄ and corrected for SiD₄ as described above (Ref. 36).

^c Rotational constants for these deuterated species obtained directly from Raghavachari (Ref. 11). These values are essentially identical to ones obtained as described above.

flux F_0 , Eq. (A8), the rotational density of states at TS0 is calculated assuming a sphere–sphere collision pair.¹³ Previous theoretical investigations of a spherical treatment for oblate/prolate tops shows this to be an excellent approximation.³⁷

The isotopic exchange process, involving TS3/C3 for $^*\text{Si}_2\text{D}_2^+$ and $^*\text{Si}_3\text{D}_4^+$ (as well as TS4/C4 for $^*\text{Si}_2\text{D}_2^+$) can also be explicitly included as described by, e.g., Eq. (A11) for $^*\text{Si}^+$. However, since these transition states and intermediate complexes are very low in energy relative to the other reaction intermediates, this is expected to make even less of an impact on the overall isotopic exchange probability $\omega_2(E, J)$ than the 0.05% change calculated for $^*\text{Si}^+$ (see Sec. IV A). Therefore, this more extensive treatment is deemed unnecessary.

In the reactions of $^*\text{Si}_2\text{D}_2^+$ and $^*\text{Si}_3\text{D}_4^+$ with SiD_4 , many of the transition states, as well as $^*\text{Si}_3\text{D}_4^+$ itself, have structures with terminal $-\text{SiD}_3$ groups. These $-\text{SiD}_3$ groups have torsional motions which are sufficiently low in frequency that at room temperature they are essentially free internal rotors. This free internal rotation affects the proper evaluation of the sum of vibrational states, Eq. (A9). The reaction involving those species with the most internal rotations is that of Si_4D_6^+ with SiD_4 to form $\text{Si}_5\text{D}_{10}^+$. As will be discussed below, proper treatment of the internal rotations changes the value calculated for the energy of the $[\text{Si}_5\text{D}_{10}^+]$ complex by only 6%. Fewer internal rotations are involved in the $^*\text{Si}_2\text{D}_2^+$ and $^*\text{Si}_3\text{D}_4^+$ reactions and the corresponding correction will be even smaller. Therefore, the full theoretical treatment of internal rotations is omitted.

3. Derivation of the probability for reaction (7)

The dissociation rate $k_D(E, J)$ in Eq. (37) can be derived from the potential surface in Fig. 10 and the molecular constants of Si_4D_6^+ , SiD_4 , and $[\text{Si}_5\text{D}_{10}^+]$. $F_0(E, J)$ is obtained from Eq. (A8) assuming a sphere–sphere collision pair for the purpose of calculating the rotational density of states (this approximation is discussed in Appendix 2 above). $\rho_{[\text{Si}_5\text{D}_{10}^+]}(E_{\text{vib}})$ is the sum of vibrational states of the activated $[\text{Si}_5\text{D}_{10}^+]$ complex with a vibrational energy, E_{vib} , less than or equal to $(E - E_2 - B_2^S J^2)$. $E - E_2$ is the depth of the well of the $[\text{Si}_5\text{D}_{10}^+]$ complex with a total system energy E ; $B_2^S J^2$ is the rotational energy [Eq. (A10)]. $F_0(E, J)$ and $\rho_{[\text{Si}_5\text{D}_{10}^+]}(E_{\text{vib}})$ are calculated using the molecular constants calculated by Raghavachari which have been corrected for deuteration.^{11,35}

As discussed above, Si_4D_6^+ and $[\text{Si}_5\text{D}_{10}^+]$ contain essentially free internal $-\text{SiD}_3$ rotors at the reaction temperature of 300 K. Each internal rotation is approximated as a motion about a symmetric top axis with relative moments of inertia I_A and I_B . The energy of this internal rotation $E_{\text{I.R.}}$ is given by^{13,35,38}

$$E_{\text{I.R.}} = B_{\text{I.R.}} K^2, \quad (\text{A12})$$

$$B_{\text{I.R.}} = \frac{h}{8\pi^2} \left(\frac{I_A + I_B}{I_A I_B} \right). \quad (\text{A13})$$

Following the assumptions used to derive Eqs. (A12) and (A13), these internal rotations can be properly treated by

removing them from the sum of vibrational states and adding them into the rotational density of states where appropriate.

- ¹G. M. Hidy, *Aerosols and Atmospheric Chemistry* (Academic, New York, 1972).
- ²(a) F. C. Eversteijn, *Philips Res. Rep.* **26**, 134 (1971); (b) T. U. M. S. Murthy, N. Miyamoto, M. Shimbo, and J. Nishizawa, *J. Crystal Growth* **33**, 1 (1976); (c) K. G. Spears, T. J. Robinson, and R. M. Roth, *IEEE Trans. Plasma Sci.* **PS-14**, 179 (1986); (d) P. Ho and W. G. Breiland, *Appl. Phys. Lett.* **44**, 51 (1984).
- ³*VLSI Technology*, edited by S. M. Sze (McGraw-Hill, New York, 1983).
- ⁴See, for example, (a) J. H. Purnell and R. Walsh, *Proc. R. Soc. London Ser. A* **293**, 543 (1966); (b) W. G. Breiland, P. Ho, and M. E. Coltrin, *J. Appl. Phys.* **60**, 1505 (1986); (c) W. G. Breiland, M. E. Coltrin, and P. Ho, *ibid.* **59**, 3267 (1986); (d) R. T. White, R. L. Espino-Rios, D. S. Rogers, M. A. Ring, and H. E. O'Neal, *Inter. J. Chem. Kinet.* **17**, 1029 (1985); (e) J. M. Jasinski and R. D. Estes, *Chem. Phys. Lett.* **117**, 495 (1985); (f) G. Inoue and M. Suzuki, *ibid.* **105**, 641 (1984); (g) C. A. DeJoseph, Jr., P. D. Haaland, and A. Garscadden, *IEEE Trans. Plasma Sci.* **PS-14**, 165 (1986); (h) F. J. Kampas and M. J. Kushner, *ibid.* **PS-14**, 173 (1986); (i) K. Enssler and S. Veprek, *Plasma Chem. Plasma Proc.* **7**, 139 (1987).
- ⁵M. J. Kushner (submitted).
- ⁶An excellent comprehensive review of this subject is given in A. W. Castleman, Jr., and R. B. Keese, *Chem. Rev.* **86**, 589 (1986).
- ⁷M. S. Foster and J. L. Beauchamp, *J. Am. Chem. Soc.* **97**, 4808 (1975).
- ⁸J. Wronka and D. P. Ridge, *J. Am. Chem. Soc.* **106**, 67 (1983).
- ⁹W. K. Meckstroth, D. P. Ridge, and W. D. Reents, Jr., *J. Phys. Chem.* **89**, 612 (1985).
- ¹⁰D. J. Fredeen and D. H. Russell, *J. Am. Chem. Soc.* **108**, 1860 (1986).
- ¹¹K. Raghavachari, *J. Chem. Phys.* **88**, 1688 (1988).
- ¹²Y. Tang, in *Reactive Intermediates*, edited by R. A. Abramovitch (Plenum, New York, 1982), Vol. 2.
- ¹³A comprehensive description of this model is given in the following articles and references therein, W. J. Chesnavich and M. T. Bowers, *Progr. React. Kinet.* **11**, 137 (1982); W. J. Chesnavich and M. T. Bowers, in *Gas Phase Ion Chemistry*, edited by M. T. Bowers (Academic, New York, 1979), Vol. 1.
- ¹⁴M. Comisarow, *Advances in Mass Spectrometry*, edited by N. R. Daly (Heyden, London, 1978); Vol. 7B.
- ¹⁵R. T. McIver, *Am. Laboratory* **1978**, 18.
- ¹⁶M. L. Mandich, V. E. Bondybey, and W. D. Reents, Jr., *J. Chem. Phys.* **86**, 4245 (1987).
- ¹⁷J. L. Beauchamp, *Annu. Rev. Phys. Chem.* **22**, 527 (1980).
- ¹⁸J. E. Bartmess and R. M. Georgiadis, *Vacuum* **33**, 149 (1983).
- ¹⁹The molecular polarizability of SiD₄ is assumed to equal that of SiH₄ which is measured to be 4.339×10^{-24} cm³; S. S. Batsonov, *Refractometry and Chemical Structure*, translated by P. P. Sutton (Consultants Bureau, New York, 1961). The empirical method of Bartmess used to calibrate the pressure introduces a margin of uncertainty in the absolute rate constants. However, since SiD₄ and CH₄ (which is used for scaling) are quite similar molecular species, the error introduced in the absolute rate constants should be negligible.
- ²⁰A value of 1.15×10^{-9} cm³ molecule⁻¹ s⁻¹ is used for the methane proton transfer rate constant which is the average of the values referenced by W. T. Huntress, Jr. and R. F. Pinizzotto, Jr., *J. Chem. Phys.* **59**, 4742 (1973).

²¹The intensity of the Si₂D₁₀⁺ product is sufficiently weak that the signals were enhanced by performing separate experiments without using isotopic labeling of any silicon atoms. Therefore, it was not possible to observe any isotope exchange. Both labeled and unlabeled Si₄D₆⁺ reactants will undergo reaction (7). For certain of the labeled *Si₄D₆⁺ isomers, isotopic exchange with SiD₄ is also expected to occur; see the theoretical discussion of this reaction, Sec. IV D, for more details.

²²The decay rate for the reaction of unlabeled Si⁺ with SiH₄ has been previously measured to be $4.8 \pm 0.6 \times 10^{-10}$ cm³ molecule⁻¹ s⁻¹, J. M. S. Henis, G. W. Stewart, M. K. Tripodi, and P. P. Gaspar, *J. Chem. Phys.* **57**, 389 (1972). This value was obtained by comparing the relative measured rate constant to a rate constant for proton transfer to CH₄ of 1×10^{-9} cm³ molecule⁻¹ s⁻¹. Recalibration of the Si⁺ decay rate is necessary in order to compare it to our measured rate constant which is derived using a somewhat revised value for the methane proton transfer reaction (Ref. 20). This yields a decay rate for unlabeled Si⁺ of $5.5 \pm 0.7 \times 10^{-10}$ cm³ molecule⁻¹ s⁻¹, as compared to our measured value (for the combined ²⁸Si⁺ and ²⁹Si⁺ populations) of $6.9 \pm 0.4 \times 10^{-10}$ cm³ molecule⁻¹ s⁻¹. While the two measurements do not quite overlap within experimental error, they are in quite reasonable agreement considering the problems encountered by early workers using drift ion cyclotron resonance techniques to measure absolute reaction rate constants.

²³B. H. Boo and P. B. Armentrout, *J. Am. Chem. Soc.* **109**, 3549 (1987).

²⁴See, for example, R. C. Dunbar, in *Molecular Ions: Spectroscopy, Structure and Chemistry*, edited by T. A. Miller and V. E. Bondybey (North-Holland, New York, 1983), W. Federer, W. Dobler, F. Howorka, W. Lindinger, M. Durup-Ferguson, and E. E. Ferguson, *J. Chem. Phys.* **83**, 1032 (1985).

²⁵W. D. Reents, Jr. and M. L. Mandich, *J. Phys. Chem.* (in press).

²⁶Details regarding the structures, energetics, etc. of the transition states and intermediate complexes in these reactions are given in Ref. 11 and are not duplicated here.

²⁷S. W. Benson, *Thermochemical Kinetics* (Wiley Interscience, New York, 1976).

²⁸E. R. Lippincott and J. M. Stutman, *J. Phys. Chem.* **68**, 2926 (1964).

²⁹D. F. McMillen and D. M. Golden, *Annu. Rev. Phys. Chem.* **33**, 493 (1982).

³⁰P. A. M. van Koppen, M. F. Jarrold, M. T. Bowers, L. M. Bass, and K. R. Jennings, *J. Chem. Phys.* **81**, 288 (1984).

³¹A reaction rate of $1.5 \pm 0.2 \times 10^{-9}$ cm³ molecule⁻¹ s⁻¹, is also obtained from the ion-beam cross sections for the reaction of Si⁺ with SiH₄. This number appears to be somewhat high since it exceeds the Langevin rate of 1.25×10^{-9} cm³ molecule⁻¹ s⁻¹ [Eq. (20)]. Note that this discrepancy is not accounted for by an isotope effect; Armentrout and Boo prefer the lower number which agrees with our results.

³²The 18 electron counting formalism is well described in J. P. Collman and L. S. Hegeudus, *Principles and Applications of Organotransition Metal Chemistry* (University Science Books, Mill Valley, 1980).

³³B. K. Teo, G. Longoni, and F. R. K. Chung, *Inorg. Chem.* **23**, 1257 (1984).

³⁴N. J. A. Sloane and B. K. Teo, *J. Chem. Phys.* **83**, 6520 (1985).

³⁵G. Herzberg, *Molecular Spectra and Molecular Structure II* (Van Nostrand Reinhold, New York, 1945).

³⁶C. H. Tindal, J. W. Straley, and H. H. Nielsen, *Phys. Rev.* **62**, 151 (1942).

³⁷W. J. Chesnavich and M. T. Bowers, *J. Chem. Phys.* **66**, 2306 (1977).

³⁸*B*_{I.R.} is computed from the geometries for Si₄D₆⁺ and [Si₂D₁₀⁺]* calculated by Raghavachari (Ref. 11). For Si₄D₆⁺, *B*_{I.R.} = 1.49 cm⁻¹ for each of two internal -SiD₃ rotors; for [Si₂D₁₀⁺]*, *B*_{I.R.} = 1.45 cm⁻¹ for each of three internal -SiD₃ rotors.